ACTIVE CLOSED LOOP CONTROL OF SUPERSONIC FLOW WITH TRANSVERSE INJECTION

by

G. V. Rajesh Kumar

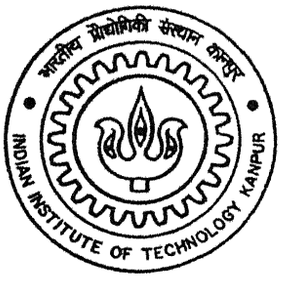

DEPARTMENT OF AEROSPACE ENGINEERING

Indian Institute of Technology Kanpur

DECEMBER, 2002

ACTIVE CLOSED LOOP CONTROL OF SUPERSONIC FLOW WITH TRANSVERSE INJECTION

A Thesis Submitted

in Partial Fulfillment of the Requirements

for the Degree of

Master of Technology

by

G. V. RAJESH KUMAR

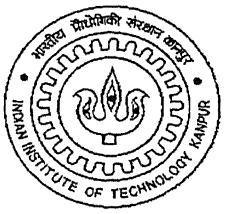

to the

DEPARTMENT OF AEROSPACE ENGINEERING

INDIAN INSTITUTE OF TECHNOLOGY KANPUR

December 2002

CERTIFICATE

It is certified that the work contained in the thesis entitled **Active Closed Loop Control of Supersonic Flow with Transverse Injection**, by **G. V. Rajesh Kumar**, has been carried out under my supervision and that this work has not been submitted elsewhere for a degree.

Dr. Ashish Tewari
Associate Professor

Department of Aerospace Engineering
Indian Institute of Technology
Kanpur

December 2002.

Dedicated to

The Great Temple of Learning

INDIAN INSTITUTE OF TECHNOLOGY, KANPUR

Acknowledgement

I feel great pleasure in expressing my sincere thanks to my thesis supervisor Dr. Ashish Tewari, who has been giving an excellent guidance and motivation throughout my thesis work. I am very grateful to him for the co-operation he has given to complete such a good thesis in time. I learned a lot from his course on 'Control Theory' and I am thankful to him for spending a lot of time in discussing the topics.

I also thank Dr. E. Rathakrishnan, Dr. K. Ghosh, Dr. R. K. Sullerey and Dr. A.K.Ghosh who handled various courses and gave the basic knowledge in Aerospace Engineering.

I found my stay at IIT Kanpur as the most memorable one in my life. This has been just possible because of my friends who had been giving the encouragement and the support needed during tough times. We had a lot of fun in Hall5 and it will be one which I will cherish throughout my life. I thank my friends Anuradha, Sridhar, Nagendra, Reddy, Ravi, Srinu, Samson, Kishore, Laxman for making my stay at IIT a pleasant one. I conclude this page by dedicating this work to this great institute which has been a temple of learning for so many years.

Contents

Abstract

A feedback control system has been designed and simulated for transverse injection into a laminar, supersonic flow over a flat plate. This control system employs the injection total pressure of nozzle as a control input to the system. Two-dimensional Navier-Stokes equations are solved with an explicit scheme to simulate the flow field. Numerical results are presented for different desired static pressure ratios and with various values of controller constants. Robustness of the controller with respect to the freestream Mach number is demonstrated. A transfer function of the linearized system is obtained from the numerical results.

List of Figures

Nomenclature

c_p -- coefficient of pressure

e -- internal energy (*Joule*)

E -- matrix containing all x derivative terms

E_t -- total energy per unit volume (*Joule/m* ^{3})

f -- acceleration vector (*m/sec* ^{2})

F -- matrix containing all y derivative terms

f_x, f_y, f_z -- acceleration along x, y and z directions respectively (*m/sec.*^{2})

g -- acceleration due to gravity (*m/sec.*^{2})

i, j -- grid point numbers along y and x axes respectively

i, j, k -- unit vectors along x, y and z directions

k -- coefficient of thermal conductivity (*Watt/m/K*)

K -- controller constant

L -- length from plate leading edge to nozzle centerline (*m.*)

M -- Mach number

p -- static pressure (N/m^2)

p_d -- desired static pressure at a specific point (N/m^2)

P_0 -- total pressure (N/m^2)

Pr -- Prandtl number

p_{sep} -- pressure in the separation region ahead of jet (N/m^2)

Q -- total heat influx per unit volume ($Watt/m^3$)

q -- rate of energy loss by convection per unit volume ($Watt/m^3$)

R -- gas constant

Re -- Reynolds number

t -- time (*sec*)

T -- static temperature (*K*)

u, v, w -- velocities along *x*, *y* and *z* directions respectively (*m/sec.*)

U -- matrix containing all time derivative terms

V -- velocity vector (*m/sec.*)

x, y -- rectangular cartesian coordinates (*m.*)

ρ -- density ($kg/m.^3$)

Π_{ij} -- stress tensor (N/m^2)

δ_{ij} -- Kronecker delta function

μ -- coefficient of viscosity ($N\,sec/m.^2$)

$\tau_{xx}, \tau_{yy}, \tau_{zz}$ -- normal stresses ($N/m.^2$)

$\tau_{xy}, \tau_{yz}, \tau_{xz}$ -- shear stresses ($N/m.^2$)

Δt -- time step (*sec.*)

γ -- specific heat ratio

Subscript

i, j -- values at *i*th and *j*th points along *y* and *x* axis respectively

jet -- jet values

0 -- total values

∞ -- freestream values

Superscript

n -- time index

Chapter 1

Introduction

1.1 Literature Survey

The significance of studying the flow field set up by normal injection of secondary gas into a supersonic primary flow has been a problem of interest because of its application in fuel injection into a supersonic combustor, thrust vector control of rocket motors and in high speed flight vehicle reaction control jets. A number of experimental studies were carried out initially to understand the complex flow field set up by normal injection into supersonic flow. Analytical and numerical studies were also been carried out to describe this complex flow field. This section gives a brief note on the various studies conducted and the advancements achieved in understanding this flow field.

Dorrance[1] studied the use of introducing a secondary fluid into a primary flow, which has a hot gas boundary layer for cooling the surface. He developed equations to study the effect of mass transfer and chemical reactions upon the laminar boundary layer properties by solving the boundary layer equations along with some chemical equations. But his theory is basically to study the effect of introducing the secondary fluid for cooling purposes.

The first experimental investigation to study the flow field set up by normal injection into supersonic flow was carried out by Spaid and Zukoski [2-3]. They conducted a series of experiments at freestream Mach numbers of 1.38 to 4.54 with gaseous nitrogen, argon and helium as injectants and proposed a scaling parameter which allows for the simple prediction of side forces generated by transverse injection. Schetz and Billing[4] studied the behaviour of gaseous jets issuing transversely into a supersonic primary stream analytically and the analysis was applied to a configuration study of a combustion chamber for a hypersonic ramjet.

George Lee [5] used the boundary layer theory along with hypersonic small disturbance theory to derive the formulas for mass-transfer distribution, pressures, heat transfer, skin friction and boundary layer displacement thickness for the hypersonic flow over a blunt flat plate with surface mass transfer. He proved that the surface pressures would be increased by mass transfer and with higher ratio of wall to stream temperature. Mass transfer will strongly influence the heat transfer and makes it to approach zero for high rates of mass transfer. Spaid and Zukoski [6] conducted flat-plate experiments with normal sonic jets at external flow Mach numbers of 2.61, 3.5 and 4.54 and developed an analytical model of the flow field by applying momentum conservation to a control volume at the jet nozzle exit. They correlated the data obtained from experiments with finite-span slots and demonstrated that the effective jet penetration height and the slot span are the important characteristic dimensions of such flowfields. Spaid [7] conducted experiments with normal, sonic jets and forward-facing steps at external flow Mach numbers of 2.5 to 13, and Reynolds number based on running length of 7.5×10^6 to 5.5×10^8.

The flow field was simulated numerically [8-13] using different turbulence models and various forms of Navier-Stokes equations. Napolitano [8] used the triple-

deck equations to solve the problem of strong slot injection into a supersonic laminar boundary layer and solved them for a wide range of wall injection velocities. Weidner and Drummond [9] solved the full two-dimensional Navier-Stokes and species equations to analyze the turbulent reacting flow field in a two-dimensional scramjet engine configurator, especially in engine inlet and combustor. They [10] also conducted a parametric study of flowfields near staged perpendicular injectors by solving the two-dimensional elliptic Navier-Stokes equations. They used MacCormack time-split algorithm with algebraic eddy-viscosity model along with a chemistry model to study the mixing phenomena of hydrogen fuel and air. They suggested the use of staged fuel injection for scramjet engine.

Rizetta [11] numerically simulated the slot injection experiments of Aso et al [12] at freestream Mach number of 3.7 with turbulence modeling simulated by eddy viscosity model. He assessed the adequacy of the turbulence model with regard to nozzle width and slot pressure ratio for jet injection flowfields. Chenault and Beran [13] studied the feasibility of compressible k-ε and second-order Reynolds-stress turbulence model for transverse injection into a supersonic flow by integrating the Favre-averaged Navier-Stokes equations. Results of his study indicated that the Reynolds-stress turbulence model correctly predicts mean flow conditions and the k-ε results are less consistent with the experimental results than those associated with the Reynolds-stress turbulence model. But the vorticity phenomena upstream of the jet were best observed with k-ε model.

While most of the above discussion is related to transverse injection into supersonic flow, there are many other applications where mass injection into external flow will be done through porous surfaces or by vectored or tangential injection. These types of injection finds application in a number of important boundary layer

flow problems such as film and transpiration cooling of rocket engines, turbine blades, surfaces of high-speed aerodynamic bodies and for skin friction reduction and boundary layer control on high-speed aircraft. The following paragraphs will give a brief note on the studies conducted in these types of flows.

Kenworthy and Schetz [14] studied the use of injection of a gas through a wall slot parallel to a supersonic stream for skin-friction reduction on high-speed aircraft. Inger and Swean [15] conducted a theoretical investigation of self-similar isobaric laminar two-dimensional boundary layer flows for a wide range of conditions for suction, as well as injection, including the effects of heat transfer. They presented detailed results for skin friction, velocity and enthalpy profiles and momentum and displacement thickness integral properties. Nilson and Tsuei [16] solved the boundary layer equations numerically by a finite difference method to study the film cooling effectiveness for oblique injection of coolant through single or multiple wall slots into a high-speed laminar flow. Schetz and vanOvereem [17] made an experimental study to compare the effectiveness of tangential slot injection and porous wall injection for skin friction reduction. Inger and Swean [18] extended their work [15] of vectored injection and suction to study the effects of self-induced pressure gradient caused by the boundary layer displacement thickness growth. They presented the results showing the effects of both injection velocity and vector angle on a variety of physical properties. Hefner [19] for the first time, conducted experiments with two different slot geometries to study whether any simple modifications to the slot configuration can produce improved cooling effectiveness and skin friction reduction. Brandies [20] numerically studied the flow field within a finite, two-dimensional slot through which fluid can either be added or subtracted and also studied the effects of the size of the slot on the flow field. Connor and Sheikh [21] conducted a computational fluid

dynamics study which focuses on injecting a heated film of air through a rearward facing slot parallel to a flat plate in a Mach 3 divergent nozzle.

Dershin et al [22] conducted an experimental investigation to calculate the skin friction on a porous plate with mass injection at a supersonic Mach number of 3.2 and with turbulent Reynolds number. But, the concentration was more on measurement of skin friction and predicted the skin friction reduction with mass injection. Thomas [23] used an inviscid, vortical flow model for analyzing the compressible flow over a finite porous plate in supersonic stream, with massive injection at a uniform rate over the surface. The above finds its application in cooling the surface during re-entry from an interplanetary mission. Clark et al [24] conducted an experimental investigation to determine the local and downstream cooling effectiveness associated with injection of water through slotted and porous surfaces into a turbulent, supersonic boundary layer. El-Mistikawy and Werle [25] developed a stable second-order accurate finite-difference scheme to provide solutions for boundary layer flows in the presence of massive injection through a porous surface.

The methods described above, i.e., transverse flow injection, parallel and vectored injection and mass injection from porous surface come under the category of active flow control where some additional input is used to get the desired effect which can be either skin-friction reduction, thrust vector control, fuel injection into supersonic combustion engine, cooling surfaces of high-speed aircraft etc. So, the interest in the active flow control for the above applications has stimulated the recent development of innovative actuator designs that create localized disturbances in a flow field. The following paragraphs will give a brief not on the recent developments achieved in actuator designs and modern flow control methods.

Nae [26] presented results for numerical simulation of synthetic jet actuator and the flow around the NACA 0012 airfoil for a given control law and for circular cylinder using active flow control. Calkins and Mabe [27] developed a synthetic jet actuator to test in a 1/10 scale V22 2D wind tunnel model and in a 1/10 scale 3D powered model. Synthetic jets result from oscillating diaphragm in an enclosed space, having small orifices at the top. The jet will be synthesized from the working fluid of the flow system requiring no external fluid source, thus they are commonly referred as zero-net-mass-transfer-flux actuators. They can be controlled electro statically or using piezo electric materials with frequencies in the range of 0.5-20 KHz. These have been found to be more effective than other traditional mechanical control systems for flow control applications. Another means of flow control can be achieved by pulsed injection. Vakili et al [28] have experimentally and numerically investigated the use of such a pulsed injection in a nozzle. Their objective was to increase the fluidic blockage produced by a transverse injector into the exhaust stream near the throat. Their experimental results depicted that the jet penetration was increased with pulsation of the jet. Also the results for various exit geometry jets indicated an improvement in the effective blockage for periodic injection compared to steady state injection.

The technique of flow control by magnetogasdynamic (MGD) forces was simulated by Gaitonde and Poggie [29]. In this, a plasma which may have been created naturally by the presence of shocks and/or artificially through some form of energy input like laser beam into the flow will be used for flow control. They developed a simulation tool by integrating the Maxwell and compressible Navier-Stokes equations with the assumptions of non-ideal magnetogasdynamics and investigated various issues concerning the numerical simulation of such a hypersonic flow control

problem. Lineberry et al [30] studied the prospects of active magneto hydrodynamic (MHD) boundary layer control and leading edge heat transfer management with MHD. They also qualitatively described MHD flow control inlet configuration concept and its operation. Also an active flow control by electro hydrodynamic (EHD) actuator was studied by Leger et al [31] for low velocity airflow along a flat plate. Such an actuator can be used to accelerate the airflow tangentially and very close to the wall, in order to modify the airflow profile within the boundary layer. Its advantage is that it directly converts electrical energy into kinetic energy without moving any mechanical part. Its response time is very short and enables a control as a function of time at high frequency. Its disadvantage is its low efficiency of energy conversion and also generation of extraneous gases such as ozone in air. Riggins and Nelson [32] numerically studied a flow control concept in which energy will be deposited at a specific point by solving the full Navier-Stokes equations. They conducted study on centerline and off-centerline power deposition at a point upstream of the two-dimensional blunt body at Mach 6.5 at 30 km. altitude. This flow control concept can be effectively used to improve the performance and to stabilize and control hypersonic vehicles.

While many experimental and numerical studies of active flow control described above have been carried out, an active flow control problem of transverse injection with a feedback has not yet been reported.

1.2 Transverse Injection into Supersonic Flow: Flow field Description

A two-dimensional flow field set up by injection of a secondary fluid normal to an external supersonic stream is shown in Fig. (1.1). In this example, it is assumed that

the jet is sonic, underexpanded and the obstruction to the external flow formed by the jet is larger than the undisturbed boundary layer thickness. Expansion of the jet occurs rapidly as it leaves the nozzle. The interaction of the secondary jet causes a strong bow shock to form upstream of the jet which provokes the boundary layer to separate. Another shock wave will be generated at the separation point, called as separation shock, which intersects the jet induced bow shock. Upon exiting the nozzle, the jet is decelerated by a normal shock, often referred as Mach disk, to obtain the pressure equilibrium. Downstream of the slot, the boundary layer reattaches resulting in a recompression shock and a subsequent separation region.

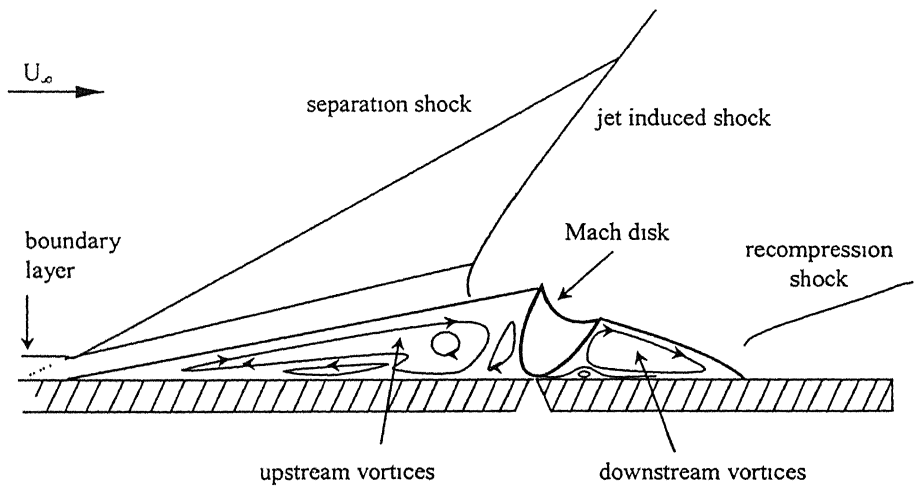

Figure1.1: Schematic of the flow field

The surface static pressure distribution for transverse injection[13] is shown in Fig. (1.2). The static pressure rises because of boundary layer separation (region 1), followed by a plateau (region 2) because of constant flow conditions of the upstream

vortices, and rises again (region 3) in the immediate vicinity of the jet because of the bow shock. Immediately downstream of the jet is a region (region 4) where both the flows will separate and pressure falls below the ambient value. This is followed by a pressure rise (region 5) because of recompression shock and boundary layer reattachment.

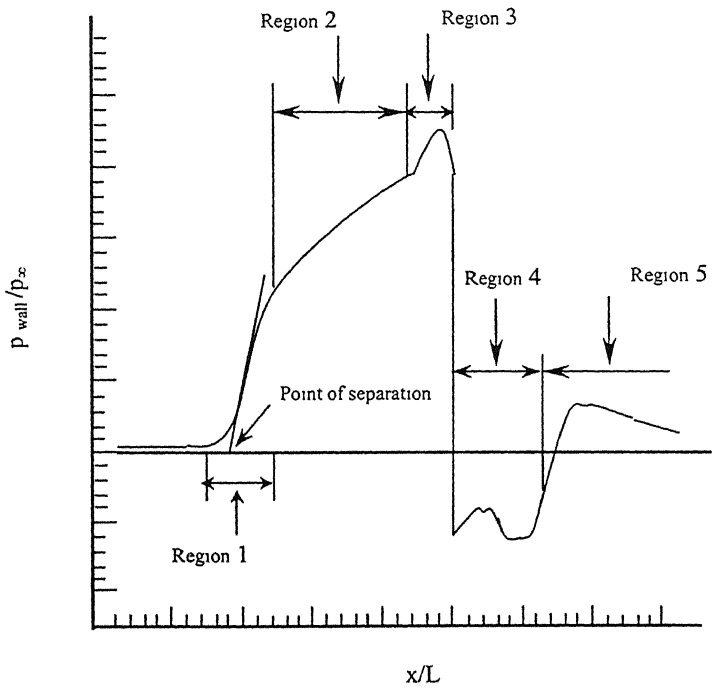

Figure 1.2: Schematic of Surface Pressure Distribution

Spaid and Zukoski [2] reported that when the boundary layer is laminar, the separation region is large and the angle between the separated flow and the wall will be very small. For the case of a turbulent boundary layer, the separation region will be small and the shock produced by separation is usually sufficiently strong to be observed.

1.3 Passive and Active Control

Passive control is a control strategy employed for a system where external inputs are not required for the control of the system. The system may be consisting of subsystems, which effectively perform the control function, without the need for distinct components for sensing and actuation. Passive flow control is normally achieved by incorporating changes in the flow geometry (e.g. introduction of fixed slots, flaps or sharp edges in the flow field)

Apart from passive control, there are control strategies which require distinct components, including actuators and sensors. This strategy is called as 'active control'. This strategy uses additional inputs for the control of the system. An active control can be either an open loop or closed loop. An open loop active control system is shown in Fig. (1.3).

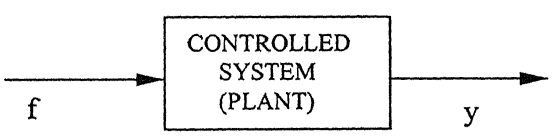

Figure 1.3: Active Control (Open loop)

The output of the above system may not be a desired output. If the controlled system's behavior is precisely known, then it is possible to achieve the desired performance through open-loop control. However, this requirement is rarely met.

Closed loop (or feed back) control is desirable if the controlled system's characteristics are unsatisfactory (such as instability, low-damping, large overshoot,

steady-state error etc.), and the closed-loop system (if properly designed) can improve the overall performance. Usually, a closed-loop system employs sensors, a feedback path, a forward path and actuators as shown in Fig. (1.4)

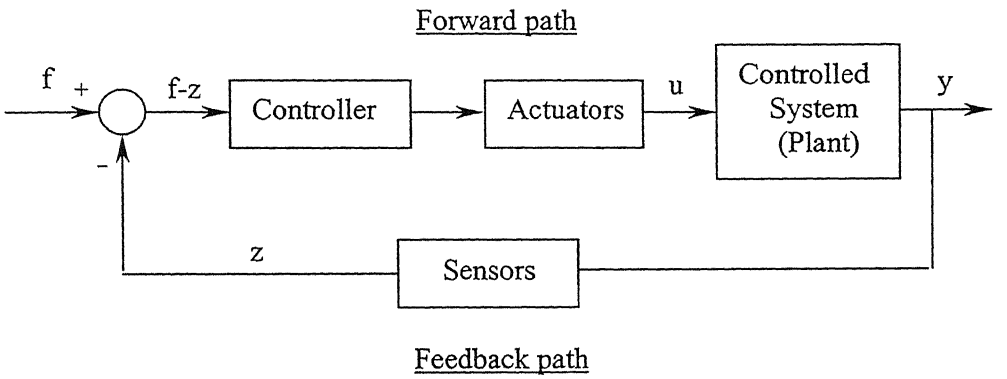

Figure 1.4: Closed loop Active control

Here, f(t) is the desired output vector, y(t) the actual output vector, z(t) the sensed output vector and u(t) the control input vector. The design of the controller must be carefully carried out to achieve the desired closed-loop performance. Modern control theory[37-39] is based upon either a transfer function or a state-space description of the controlled system (plant), and is largely restricted to linear systems. However, most non-linear systems can be linearized about their equilibrium points, and thus the concepts of modern control theory can be applied to design a controller for non-linear systems where only small deviations from an equilibrium point are expected. This is the approach adopted in the present thesis, where the plant is described by nonlinear

partial differential equations (Navier-Stokes equations) and linearized transfer function approximation is used for designing the controller.

1.4 Types of Feedback Controllers

The commonly used feedback controllers for SISO plants are

1. Proportional controller
2. Integral controller
3. Proportional-plus-Integral controller
4. Derivative controller
5. Proportional-plus-Derivative controller
6 Proportional-plus-Integral-plus-Derivative controller

1.4.1 PID controller

The transfer function of a PID controller is of the form

$$\frac{U(s)}{E(s)} = K_p + K_d s + \frac{K_i}{s} \qquad (1.1)$$

and its block diagram is shown in Fig. (1.5)

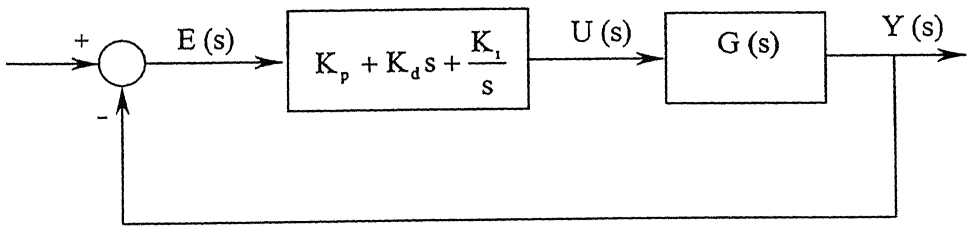

Figure 1.5: Block Diagram of a PID Controller

where $U(s) = \mathcal{L}\{ u(t) \}$, $E(s) = \mathcal{L}\{ e(t) \}$, $Y(s) = \mathcal{L}\{ e(t) \}$

u(t) is the control input, y(t) is the output and e(t) is the error signal. G(s) is the plant's transfer function and K_p, K_d and K_i are constants. The integral term, K_i/s, introduces a pole at s=0, thus increasing the type of the closed loop system by one. This reduces the steady state error of the original system. The proportional term K_p, and derivative term, $K_d s$, can be used to improve the transient response of the system by placing two zeros at suitable locations. They can be made to yield a system with fast rise time and with little or no overshoot because of increased system damping. Thus a PID controller will have the advantages of all the three controllers and thus can be used to improve both the transient and steady state response of the system.

Chapter 2

Active Control Strategy and Governing Equations

2.1 Formulation of Navier-Stokes Equations

2.1.1 Continuity Equation

The conservation of mass law applied to a perfect gas passing through an infinitesimal, fixed control volume yields the following equation of continuity

$$\frac{\partial \rho}{\partial t} + \nabla \cdot (\rho \, \mathbf{V}) = 0 \tag{2.1}$$

The first term in this equation represents the rate of increase of the density in the control volume and the second term represents the rate of mass flux passing out of the control surface (which surrounds the control volume) per unit volume.

For a Cartesian coordinate system, where u, v, w represent the x, y, z components of the velocity vector **V**, the above equation becomes

$$\frac{\partial \rho}{\partial t} + \frac{\partial (\rho u)}{\partial x} + \frac{\partial (\rho v)}{\partial y} + \frac{\partial (\rho w)}{\partial z} = 0 \tag{2.2}$$

2.1.2 Momentum Equation

Newton's second law applied to a perfect gas passing through an infinitesimal, fixed control volume yields the following momentum equation

$$\rho \frac{D\mathbf{V}}{Dt} = \rho \mathbf{f} - \nabla p + \frac{\partial}{\partial x_j}\left[\mu\left(\frac{\partial u_i}{\partial x_j} + \frac{\partial u_j}{\partial x_i}\right) - \frac{2}{3}\delta_{ij}\,\mu\frac{\partial u_k}{\partial x_k}\right] \qquad (2.3)$$

or

$$\rho \frac{D\mathbf{V}}{Dt} = \rho \mathbf{f} - \nabla p + \frac{\partial}{\partial x_j}\left[\tau_{ij}\right] \qquad (i, j, k = 1, 2, 3) \qquad (2.4)$$

where τ_{ij} is the viscous stress tensor and δ_{ij} is the Kronecker delta function (δ_{ij} =1 if i = j and δ_{ij} = 0 if i ≠ j); u_1, u_2, u_3 represent the three components of the velocity vector **V**; x_1, x_2, x_3 represent the three components of the position vector.

The first term on the right-hand side of the above equation is the body force per unit volume. Body forces act at a distance and apply to the entire mass of the fluid. The most common body force is the gravitational force. In this case, the force per unit mass (**f**) equals the acceleration due to gravity vector **g**

$$\rho \mathbf{f} = \rho \mathbf{g} \qquad (2.5)$$

The second and third term on the right-hand side represents the surface forces per unit volume. These forces are applied by the external stresses on the fluid element. The stresses consist of normal stresses and shearing stresses.

For a Cartesian coordinate system, the Navier-Stokes equations can be written in conservation-law form as

$$\begin{aligned}
&\frac{\partial(\rho u)}{\partial t} + \frac{\partial}{\partial x}\left(\rho u^2 + p - \tau_{xx}\right) + \frac{\partial}{\partial y}\left(\rho uv - \tau_{xy}\right) + \frac{\partial}{\partial z}\left(\rho uw - \tau_{xz}\right) = \rho f_x \\
&\frac{\partial(\rho v)}{\partial t} + \frac{\partial}{\partial x}\left(\rho uv - \tau_{xy}\right) + \frac{\partial}{\partial y}\left(\rho v^2 + p - \tau_{yy}\right) + \frac{\partial}{\partial z}\left(\rho vw - \tau_{yz}\right) = \rho f_y \qquad (2.6) \\
&\frac{\partial(\rho w)}{\partial t} + \frac{\partial}{\partial x}\left(\rho uw - \tau_{xz}\right) + \frac{\partial}{\partial y}\left(\rho vw - \tau_{yz}\right) + \frac{\partial}{\partial z}\left(\rho w^2 + p - \tau_{zz}\right) = \rho f_z
\end{aligned}$$

where the components of the viscous stress tensor τ_{ij} are given by

$$\tau_{xx} = \frac{2}{3}\mu\left(2\frac{\partial u}{\partial x} - \frac{\partial v}{\partial y} - \frac{\partial w}{\partial z}\right)$$

$$\tau_{yy} = \frac{2}{3}\mu\left(2\frac{\partial v}{\partial y} - \frac{\partial u}{\partial x} - \frac{\partial w}{\partial z}\right)$$

$$\tau_{zz} = \frac{2}{3}\mu\left(2\frac{\partial w}{\partial z} - \frac{\partial u}{\partial x} - \frac{\partial v}{\partial y}\right)$$

$$\tau_{xy} = \mu\left(\frac{\partial u}{\partial y} + \frac{\partial v}{\partial x}\right) = \tau_{yx}$$

$$\tau_{xz} = \mu\left(\frac{\partial w}{\partial x} + \frac{\partial u}{\partial z}\right) = \tau_{zx}$$

$$\tau_{yz} = \mu\left(\frac{\partial v}{\partial z} + \frac{\partial w}{\partial y}\right) = \tau_{zy} \qquad (2.7)$$

and

$$\mathbf{f} = f_x\,\mathbf{i} + f_y\,\mathbf{j} + f_z\,\mathbf{k} \qquad (2.8)$$

where **i**, **j**, and **k** are unit vectors along x, y and z directions respectively.

2.1.3 Energy Equation

The first law of thermodynamics applied to a perfect gas passing through an infinitesimal, fixed control volume yields the following energy equation

$$\frac{\partial E_t}{\partial t} + \nabla \cdot E_t\mathbf{V} = \frac{\partial Q}{\partial t} - \nabla \cdot \mathbf{q} + \rho\mathbf{f} \cdot \mathbf{V} + \nabla \cdot \left(\Pi_{ij} \cdot \mathbf{V}\right) \qquad (2.9)$$

where E_t is the total energy per unit volume given by

$$E_t = \rho\left(e + \frac{V^2}{2} + \ldots\right) \qquad (2.10)$$

$$V^2 = u^2 + v^2 + w^2 \tag{2.11}$$

and Π_{ij} is the stress tensor given by

$$\Pi_{ij} = -p\delta_{ij} + \mu\left[\left(\frac{\partial u_i}{\partial x_j} + \frac{\partial u_j}{\partial x_i}\right) - \frac{2}{3}\delta_{ij}\frac{\partial u_k}{\partial x_k}\right] \quad (i, j, k = 1, 2, 3) \tag{2.12}$$

The first term on the left-hand side of the energy equation represents the rate of increase of total energy per unit volume in the control volume while the second term represents the rate of total energy lost by convection (per unit volume) through the control surface.

The first term on the right-hand side of the equation is the rate of heat produced per unit volume by external agencies while the second term is the rate of heat lost by conduction (per unit volume) through the control surface. The third term represents the work done on the control volume (per unit volume) by the body forces while the fourth term represents the work done on the control volume (per unit volume) by the surface forces.

For a Cartesian coordinate system, equation becomes

$$\begin{aligned}\frac{\partial E_t}{\partial t} - \frac{\partial Q}{\partial t} - \rho\left(f_x u + f_y v + f_z w\right) + \frac{\partial}{\partial x}\left(E_t u + pu - u\tau_{xx} - v\tau_{xy} - w\tau_{xz} + q_x\right) \\ + \frac{\partial}{\partial y}\left(E_t v + pv - u\tau_{xy} - v\tau_{yy} - w\tau_{yz} + q_y\right) \\ + \frac{\partial}{\partial z}\left(E_t w + pw - u\tau_{xz} - v\tau_{yz} - w\tau_{zz} + q_z\right) = 0\end{aligned} \tag{2.13}$$

which is in conservation-law form.

$$\mathbf{q} = q_x\mathbf{i} + q_y\mathbf{j} + q_z\mathbf{k} \tag{2.14}$$

In terms of heat conduction

$$q_x = -k\left(\frac{\partial T}{\partial x}\right)$$

$$q_y = -k\left(\frac{\partial T}{\partial y}\right)$$

$$q_z = -k\left(\frac{\partial T}{\partial z}\right) \tag{2.15}$$

2.1.4 Vector Form of Equations

The governing equations for application of finite difference algorithm were taken to be two-dimensional unsteady, compressible Navier-Stokes equations without body forces, external heat addition or turbulence model Written in conservation form in Cartesian rectangular coordinates, these equations can be expressed as

$$\frac{\partial \mathbf{U}}{\partial t} + \frac{\partial \mathbf{E}}{\partial x} + \frac{\partial \mathbf{F}}{\partial y} = 0 \tag{2.16}$$

where

$$\mathbf{U} = \begin{bmatrix} \rho \\ \rho u \\ \rho v \\ E_t \end{bmatrix}$$

$$\mathbf{E} = \begin{bmatrix} \rho u \\ \rho u^2 + p - \tau_{xx} \\ \rho u v - \tau_{xy} \\ (E_t + p)u - u\tau_{xx} - v\tau_{xy} + q_x \end{bmatrix}$$

$$\mathbf{F} = \begin{bmatrix} \rho v \\ \rho u v - \tau_{yx} \\ \rho v^2 + p - \tau_{yy} \\ (E_t + p)v - u\tau_{xy} - v\tau_{yy} + q_y \end{bmatrix} \tag{2.17}$$

where $$E_t = \rho\left(e + \frac{V^2}{2}\right)$$

$$\tau_{xx} = \frac{2}{3}\mu\left(2\frac{\partial u}{\partial x} - \frac{\partial v}{\partial y}\right)$$

$$\tau_{yy} = \frac{2}{3}\mu\left(2\frac{\partial v}{\partial y} - \frac{\partial u}{\partial x}\right)$$

$$\tau_{xy} = \mu\left(\frac{\partial u}{\partial y} + \frac{\partial v}{\partial x}\right) = \tau_{yx}$$

and Sutherland's law for viscosity coefficient

$$\mu = \mu_0 \left(\frac{T}{T_0}\right)^{\frac{3}{2}} \frac{T_0 + 110}{T + 110} \tag{2.18}$$

and the perfect gas relationship for calculation of pressure have been employed. The thermal conductivity was calculated from

$$k = \frac{\mu\, C_p}{\mathrm{Pr}} \tag{2.19}$$

2.2 Boundary Conditions

The boundary conditions specified for the computational domain are as follows

1. At the leading edge of the plate

$$\begin{aligned} u &= 0 \\ v &= 0 \\ p &= p_\infty \\ T &= T_\infty \end{aligned} \tag{2.20}$$

2. At the inflow boundary (except the leading edge) and upper boundaries

$$\begin{aligned} u &= V_\infty \\ v &= 0 \\ p &= p_\infty \\ T &= T_\infty \end{aligned} \tag{2.21}$$

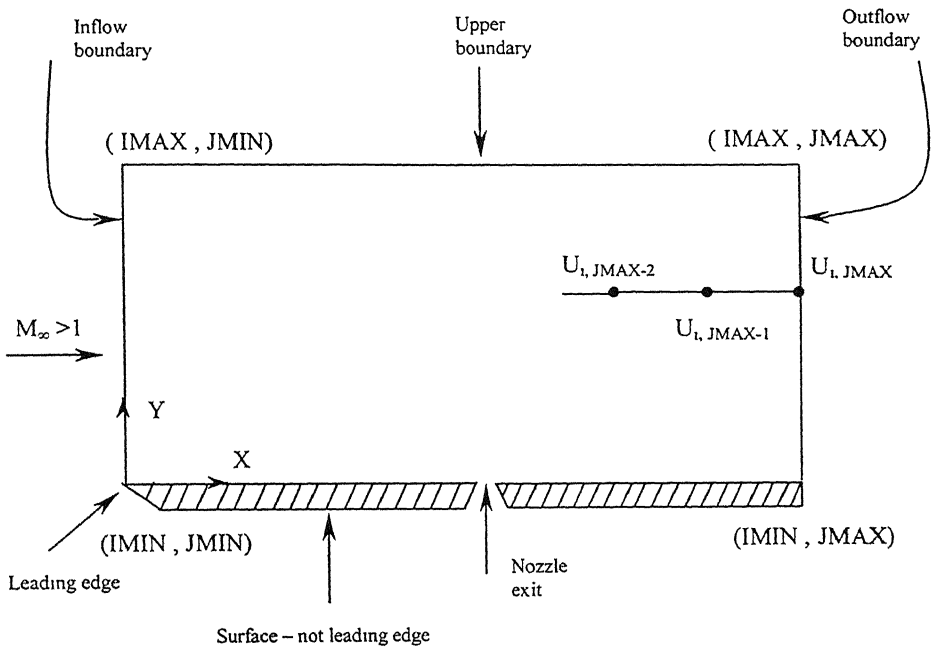

Figure 2.1: Application of Boundary Condition

3. All the properties on the outflow boundary (except i = 0 and i = IMAX) are calculated based on an extrapolation from the two interior points, at the same i location. For example, u is determined as follows

$$u_{(i, JMAX)} = \left(2\, u_{(i, JMAX-1)}\right) - u_{(i, JMAX-2)} \tag{2.22}$$

4. On the lower wall, the no-slip condition (u = v = 0) is specified on velocity along with

$$\frac{\partial p}{\partial n} = 0 \tag{2.23}$$

and adiabatic wall condition

$$\frac{\partial T}{\partial n} = 0 \tag{2.24}$$

5. At the nozzle exit

$$\begin{aligned} u &= 0 \\ v &= v_{jet} \\ p &= p_{jet} \\ T &= T_{jet} \end{aligned} \tag{2.25}$$

2.3 Active Control Strategy for Transverse Injection

The boundary conditions used for designing a controller employ the strategy of active control. An active control system will give the desired input as compared to a 'passive control system', where the output of the system may not be the desired one. The feedback control system used is shown in Fig. (2.2)

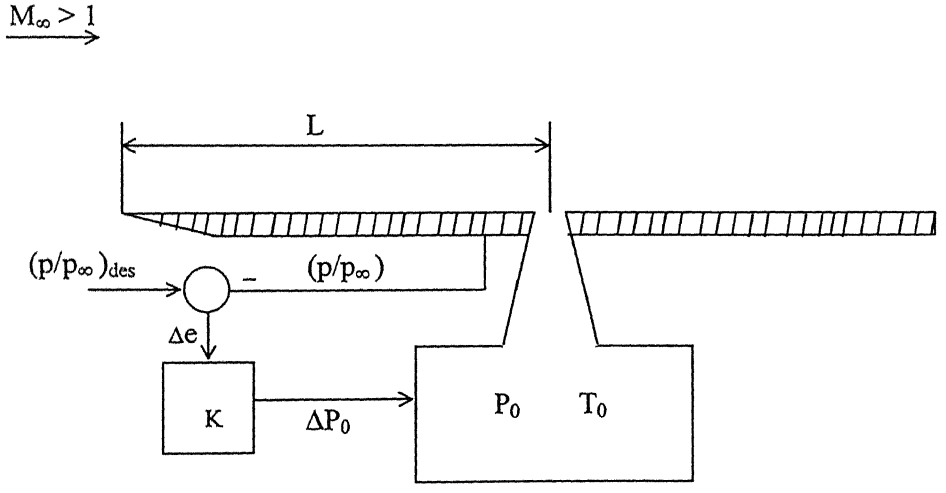

Figure 2.2: Schematic of Slot Injection Geometry with Control System

where $$\Delta e = \left(\frac{p}{p_\infty}\right)_{des} - \left(\frac{p}{p_\infty}\right) \tag{2.26}$$

is the error in the pressure ratio at a specific point and K is the controller gain.

The control input to the plant is the change in total pressure that is calculated from

$$P_0^{n+1} - P_0^n = \Delta P_0 = K(\Delta e) \tag{2.27}$$

The new P_0 and T_0 (held constant) are used to calculate the properties of secondary jet stream. Assuming the flow in the nozzle to be isentropic

$$M_{jet} = \sqrt{\left(\frac{2}{\gamma - 1}\right)\left[\left(\frac{P_0}{p_e}\right)^{\frac{\gamma-1}{\gamma}} - 1\right]} \tag{2.28}$$

where $p_e = p_{sep}/2$ [Ref. 4] (2.29)

where p_e is the exit pressure of nozzle and p_{sep} is the separation pressure, which is evaluated at a grid point just before the slot.

$$T_{jet} = \frac{T_0}{\left(1 + \frac{\gamma - 1}{2} M_{jet}^2\right)} \tag{2.30}$$

$$v_{jet} = M_{jet} \sqrt{\gamma R T_{jet}} \tag{2.31}$$

$$p_{jet} = \frac{P_0}{\left(1 + \frac{\gamma - 1}{2} M_{jet}^2\right)^{\frac{\gamma}{\gamma-1}}} \tag{2.32}$$

T_{jet}, v_{jet}, p_{jet} are the jet values at the nozzle exit. These are specified as the boundary conditions at the slot exit along with u = 0.At the start of iteration p_e and p_{jet} will not be equal. They will be changing from iteration to iteration and becomes equal when the solution reaches the steady state.

Chapter 3

Numerical Solution Procedure for Transverse Injection

3.1 Numerical Solution of Navier-stokes Equations

The finite difference method has been used to solve the governing flow equations presented in Chapter 2. The partial differential equations are converted to difference equations by discretization of governing equations on a finite grid. The flow field variables are evaluated at each node and after each time step.

3.1.1 Discretization of Derivatives

Each term of governing partial differential equations can be written in a finite difference form using taylor series expansion. For example, referring to Fig. (3.1)

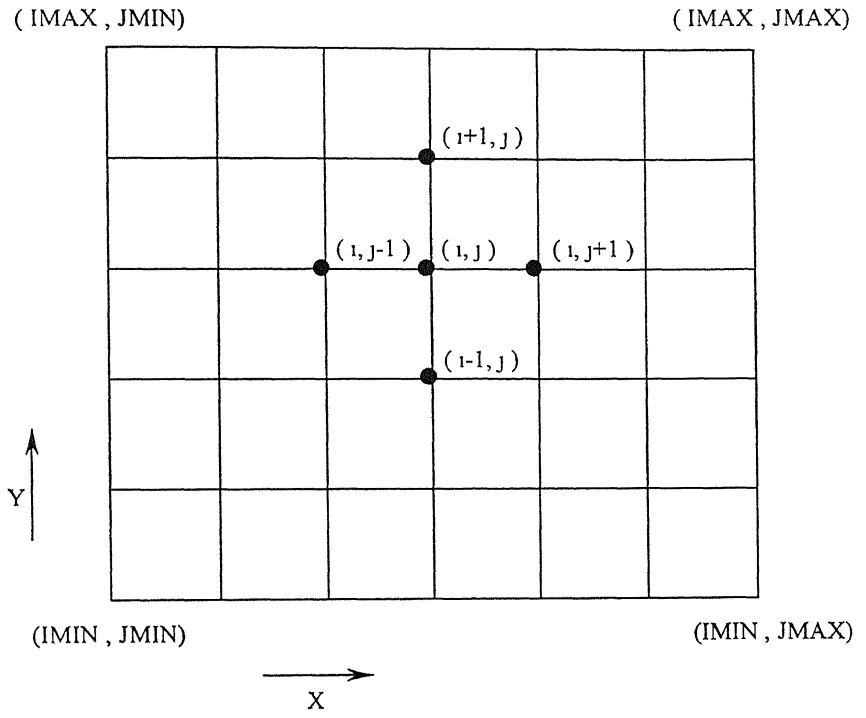

Figure 3.1: Finite Difference Grid Representation

$$\left(\frac{\partial u}{\partial y}\right)_{(i,j)} = \frac{u_{i+1,j} - u_{i,j}}{y_{i+1} - y_i} \quad (\textit{Forward difference})$$

$$= \frac{u_{i,j} - u_{i-1,j}}{y_i - y_{i-1}} \quad (\textit{Backward difference}) \qquad (3.1)$$

$$= \frac{u_{i+1,j} - u_{i-1,j}}{y_{i+1} - y_{i-1}} \quad (\textit{Central difference})$$

3.1.2 Grid Generation

Uniform and non-uniform grids are used to obtain the results. Fig. (3.2) shows the grid geometries used to get the results. Non-uniform grid in Fig. (3.2B) can be used to resolve the boundary layer more clearly by including a finer grid near the wall and a

coarser grid near the upper boundary. The following transformation[36] is used to get the stretching in the y direction.

$$y[i] = H \frac{(a+1)-(a-1)\left(\frac{a+1}{a-1}\right)^{1-y1[i]}}{\left(\frac{a+1}{a-1}\right)^{1-y1[i]}+1} \tag{3.2}$$

Here 'a' is the parameter to check the fineness at the wall. As 'a' approaches '1' more grid points are clustered near the surface.

The grid in Fig. (3.2C) is used to resolve the near wall effects around the secondary jet. The following transformation[36] is used to get the stretching.

$$x[j] = D\left[1+\frac{Sinh\left(b(x1[j]-A)\right)}{Sinh\left(bA\right)}\right] \tag{3.3}$$

where

$$A = \frac{1}{2b}\ln\left[\frac{1+\left(e^{b}-1\right)\left(\frac{D}{L}\right)}{1+\left(e^{-b}-1\right)\left(\frac{D}{L}\right)}\right] \tag{3.4}$$

'D' is the length from the leading edge of the plate where clustering is required and b = 0 to ∞, is the parameter to check the fineness. When b = 0, no clustering will be enforced. L and H are the horizontal and vertical lengths of the computational domain respectively.

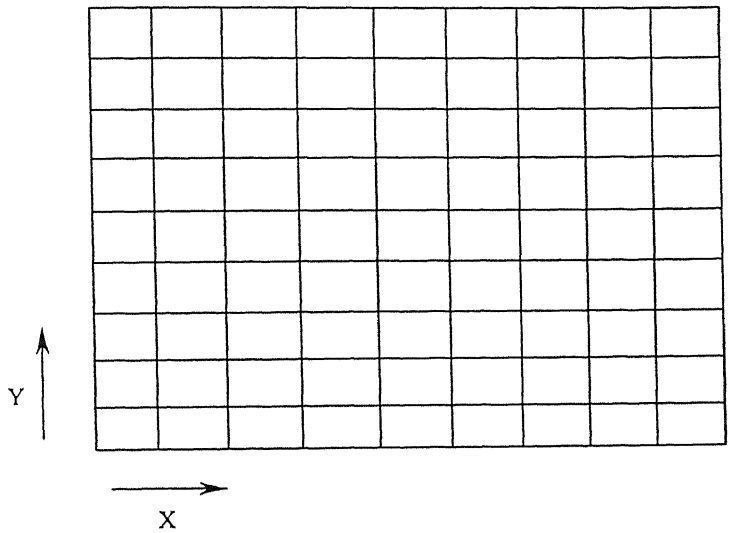

(A) UNIFORM GRID (10 × 10)

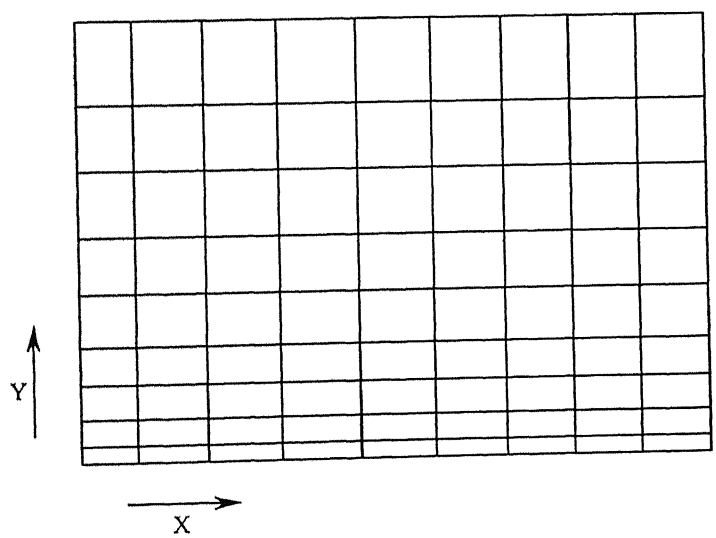

(B) NON-UNIFORM GRID (10 × 10)

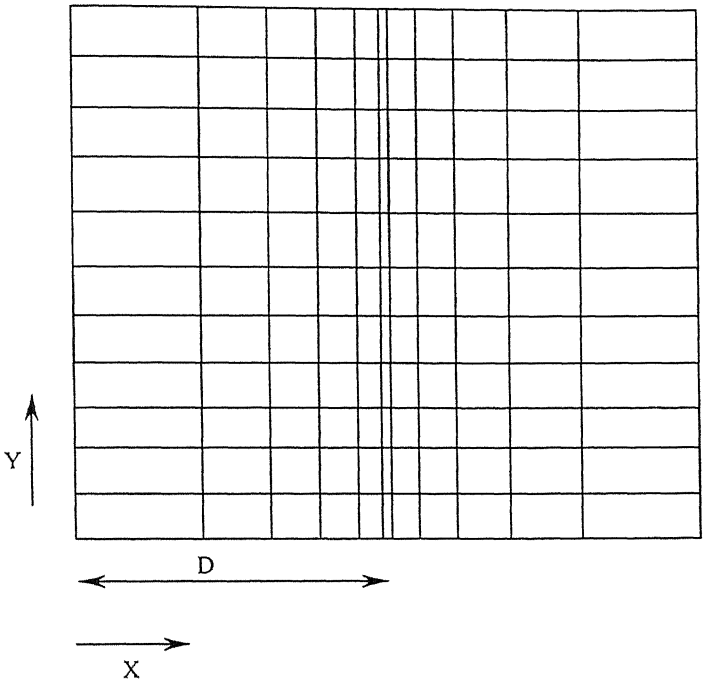

(C) NON-UNIFORM GRID (12 × 12)

Figure 3.2: Uniform and Non-Uniform Grid Geometry

3.1.3 MacCormack Scheme

The governing equation (2.16) is rewritten in vector notation as

$$\frac{\partial \mathbf{U}}{\partial t} = -\frac{\partial \mathbf{E}}{\partial x} - \frac{\partial \mathbf{F}}{\partial y} \tag{3.5}$$

Steady state solution to the above equation was obtained using the time-dependent explicit two-step predictor-corrector finite difference algorithm of MacCormack, which has been proved to be a dependable technique for producing numerical solutions to wide variety of complex fluid flow problems.

The flow field variables are advanced at each grid point (i, j) in steps of time as

$$\mathbf{U}_{i,j}^{t+\Delta t} = \mathbf{U}_{i,j}^{t} + \left(\frac{\partial \mathbf{U}}{\partial t}\right)_{av} \Delta t \tag{3.6}$$

where $$\left(\frac{\partial \mathbf{U}}{\partial t}\right)_{av} = \frac{1}{2}\left[\left(\frac{\partial \mathbf{U}}{\partial t}\right)_{i,j}^{t} + \left(\frac{\overline{\partial \mathbf{U}}}{\partial t}\right)_{i,j}^{t+\Delta t} \right] \tag{3.7}$$

is the average of derivative values of **U** of predictor and corrector steps.

After each predictor or corrector step, the physical variables are obtained from vector **U** as follows

$$\begin{aligned}
\rho_{i,j} &= \mathbf{U}_1 \\
u_{i,j} &= \frac{\mathbf{U}_2}{\mathbf{U}_1} \\
v_{i,j} &= \frac{\mathbf{U}_3}{\mathbf{U}_1} \\
E_{t\,i,j} &= \mathbf{U}_4 \\
e_{i,j} &= \frac{\mathbf{U}_4}{\mathbf{U}_1} - \frac{u_{i,j}^{\,2} + v_{i,j}^{\,2}}{2}
\end{aligned} \tag{3.8}$$

Having obtained $\rho_{i,j}$, $u_{i,j}$, $v_{i,j}$ and $e_{i,j}$, the remaining flow field variables can be obtained as follows

$$\begin{aligned}
T_{i,j} &= \frac{e_{i,j}}{c_v} \\
p_{i,j} &= \rho_{i,j} R T_{i,j} \\
\mu_{i,j} &= \mu_0 \left(\frac{T_{i,j}}{T_0}\right)^{\frac{3}{2}} \frac{T_0 + 110}{T_{i,j} + 110} \\
k_{i,j} &= \frac{\mu_{i,j} c_p}{\mathrm{Pr}}
\end{aligned} \tag{3.9}$$

3.1.4 Discretization of Boundary Conditions

The x derivatives on the inflow boundary are obtained by forward difference and on the outflow boundary by backward difference. Similarly the y derivatives on the plate surface are obtained by forward difference and that on the upper boundary by backward difference. For example, on plate surface

$$\left(\frac{\partial u}{\partial y}\right)_{(0,j)} = \frac{u_{1,j} - u_{0,j}}{y[1] - y[0]} \tag{3.10}$$

The value of p_{sep} is calculated by extrapolation from the two interior points

$$p_{sep} = 2 \times p[1][j] - p[2][j] \tag{3.11}$$

3.1.5 Calculation of Time Step

Because of the explicit nature of the procedure, a time step-size limitation exists for stability. The time step-size is calculated from Courant-Friedrichs-Lewy (CFL) criterion[35] and is given by

$$(\Delta t_{CFL})_{i,j} = \left[\frac{|u_{i,j}|}{\Delta x} + \frac{|v_{i,j}|}{\Delta y} + a_{i,j}\sqrt{\frac{1}{\Delta x^2} + \frac{1}{\Delta y^2}} + 2\nu'\left(\frac{1}{\Delta x^2} + \frac{1}{\Delta y^2}\right)\right]^{-1} \tag{3.12}$$

where
$$\nu' = \max\left[\frac{\frac{4}{3}\mu_{i,j}\left(\gamma\,\mu_{i,j}/\mathrm{Pr}\right)}{\rho_{i,j}}\right] \tag{3.13}$$

and the time step

$$\Delta t = \min\left[K_f\left((\Delta t_{CFL})_{i,j}\right)\right] \tag{3.14}$$

for $0.5 \le K_f \le 0.8$ .K_f acts as a 'fudge factor', to make the solution stable.

3.2 Solution Procedure

The steady state solution of the flat plate is taken as the initial condition. Boundary conditions for the jet are obtained from control strategy and MacCormack scheme is applied to calculate the flow field variables at the next time step. The procedure can be summarized as follows

1. Initialize the variables u, v, p and T at all the grid points obtained from the steady state solution.

2. Find the other variables ρ, E_t, e, μ and k using the present value of u, v, p and T

3. Calculate the time step by the CFL criterion.

4.Calculate the flow field variables after the predictor step using MacCormack scheme.

5. Get the jet boundary conditions from the control strategy.

6. Apply the boundary conditions.

7. Repeat steps 4, 5 and 6 for the corrector step.

8. Repeat the above steps until steady state is reached.

Chapter 4

Results and Discussions

The system used for computations is SG3400 workstation of IIT kanpur computer center. The program converges in 20 minutes for a grid of 70 × 70 for 8000 iterations.

4.1 Validation of the code

The qualitative validation of the code developed is done by comparing the computed surface pressure distribution with that shown in Ref. [13]. The computed surface pressure distribution in Fig. (4.1) shows a pressure rise because of separation shock followed by another pressure rise because of bow shock. Also the pressure fall because of separation downstream of jet and a pressure rise because of recompression shock can also be seen. The geometry selected for comparison consists of a slot of width w=0.0189 L. The freestream values are taken to be T=288.16 K, p=101325 N/m^2. The Reynolds number based on L is approximately 65500 and an uniform grid of 376×182 has been taken to make the comparison

4.2 Results of closed loop control study

The configuration selected for control system study consists of a flat plate of length '2L'. The width of the nozzle at the slot exit is w=0.15L.The freestream values are taken as T=288.16 K, p=101325 N/m^2 This has been selected because it gives laminar flow over the entire flat plate with Reynolds number about 1000 so that computational running times are short as compared to high Reynolds number applications. The study has been performed for Mach numbers 3.5 to 4.5 The primary and secondary fluids are assumed to be air.

The result in Figs. (4.2) to (4.5) shows the numerical experimentation done to design the controller for different desired pressure ratios. In Fig. (4.2), for a desired pressure ratio of 3.0, the controller values of 2.0 and 10.0 were not able to give the desired pressure ratio. A minimum value of K=30 is required to get the desired pressure ratio of 3.0. Similarly in Fig. (4.3), the controller values of 10.0 and 30.0 were not able to give the desired pressure ratio of 4.0. A minimum value of K=50 is required to get the desired pressure ratio of 4.0. Likewise, a minimum value of K=100 and K=200 are required for desired pressure ratios of 5.0 and 7.0 respectively and are shown in Figs. (4.4) and (4.5). A value of K=100 can be the best one, to use for desired pressure ratios upto 5.0 for M=4.0, as more stagnation pressure will not be required in the transient state. A value of K=200 will be the best one for desired pressure ratios upto 7.0. But, the injection total pressure can be very high in the transient state for low desired pressure ratios.

Figs. (4.6) to (4.9) shows the plots of desired output, the control input, injection Mach number and injection pressure variation with time for different values of K and M=4.0. As can be seen from the plots that with increase in the value of K, more injection stagnation pressure is required in the transient state, thus making the

flow to get choked for sometime, though the nozzle doesn't need to be choked in the steady state. This is the advantage of using an active feedback control system, as for some cases of desired pressure ratios, it only requires an unchoked flow to get the desired pressure ratio. This is not the case with an open-loop control, used in all the references where they always used a choked flow.

Fig. (4.10) shows the results for M=4.0 and K=200 for different desired pressure ratios. From Fig. (4.10b), for same freestream Mach number, in order to get a higher desired pressure ratio, the injection total pressure has to be increased. A higher injection total pressure means a greater secondary mass flow rate, thus increasing the strength of bow shock wave, which gives a greater pressure rise downstream of the shock. As can be seen from Fig. (4.10c), the nozzle was not choked when desired pressure ratio was 4.0. But when the desired pressure ratio was 7.0 the nozzle gets choked, thus indicating a greater secondary mass flow required to get a higher desired pressure ratio. Though the nozzle was choked, increasing the injection total pressure can increase the mass flow rate.

Fig. (4.11) shows the variation of different quantities with changes in Mach number. These plots can also be used to study the robustness of this control system to changes in input quantities, in particular freestream Mach number, which is always possible in a physical situation. From the plots it can be said that the control system will give the desired steady state even when there are slight changes in input quantities. Though the control system was designed for M=4.0, it can sustain changes in Mach number from 3.5 to 4.5 for a desired pressure ratio of 4.0 and K=100. From Fig. (4.11c), we can see that for the same desired pressure ratio, for a smaller freestream Mach number, we need a greater injection Mach number and stagnation pressure indicating a greater secondary mass flow rate.

Figs. (4.12) to (4.15) shows the Mach number contours for a transient and steady state for M=4.0, $p_d / p_\infty = 4.0$ and K=100. The separation regions before and after the slot can be seen from contours. Figs (4.14) and (4.15) shows the Mach number contours near the slot for a transient time and steady state. Fig. (4.15) shows the increase in the separation region as the solution reaches the steady state. Shear stress contours are shown in Fig. (4.16) and temperature contours in Fig. (4.17) respectively for M=4.0, $p_d / p_\infty = 4.0$ and K=100. Fig. (4.18) shows the surface pressure distribution for a uniform and non-uniform grid of 70×70. The non-uniformity is employed only in y-direction (a=2) with a uniform grid in x-direction. Increasing the fineness near the wall by employing a non-uniform grid shows that, the separation regions can be best captured. Also the non-uniform grid shows a higher pressure rise because of leading edge shock wave as more grid points are employed near the wall. Fig. (4.19) shows the comparison between a uniform and non-uniform grid of 70×70 with non-uniformity employed only in x-direction. The plots shows that by employing more grid points before and after the slot, the separation regions can be captured more clearly.

4.3 Identification of System Transfer Function

The governing flow equations (Navier-Stokes) are of non-linear nature. We have to make some drastic approximations to make the equations linear about an equilibrium point in order to get the transfer function of the system. This is not a practical way of getting the transfer function of the system. Instead the modeling of such complex systems about an equilibrium point can be done by using techniques of modern control theory. This type of modeling can be done based on the input-output relationship of the system. The time histories of the output (desired pressure ratio) and

input (injection total pressure) are used to model the system by transforming them into the frequency domain and the resulting frequency responses are used to obtain the transfer function. Fast Fourier transform was used to transform the time history data of input and output to the frequency domain assuming the system to be linear.

Assuming the differential equation associated with the system to be linear, the fast fourier transform of input and output was plotted for different Mach numbers and is shown in Fig. (4.20) for $p_d / p_\infty = 4.0$ and K=100. Fast Fourier transform was obtained using MATLAB and the frequency vector used to get the fast fourier transform was taken from page 327 of Ashish Tewari [39]. The approximate transfer function of the system for M=4.0 was obtained as

$$G(s) = \frac{3.1078 \times 10^{-5} s^2 + 2.7 \times 10^5 s + 3.2563 \times 10^{13}}{s^2 + 8.2901 \times 10^9 s + 1.8714 \times 10^{18}} \qquad (4.1)$$

that suits best in the frequency range $10^8 < \omega < 10^{11}$ .The comparison between the exact and approximate frequency response is shown in Fig. (4.21). This transfer function can be used to improve the system performance by designing a PID controller.

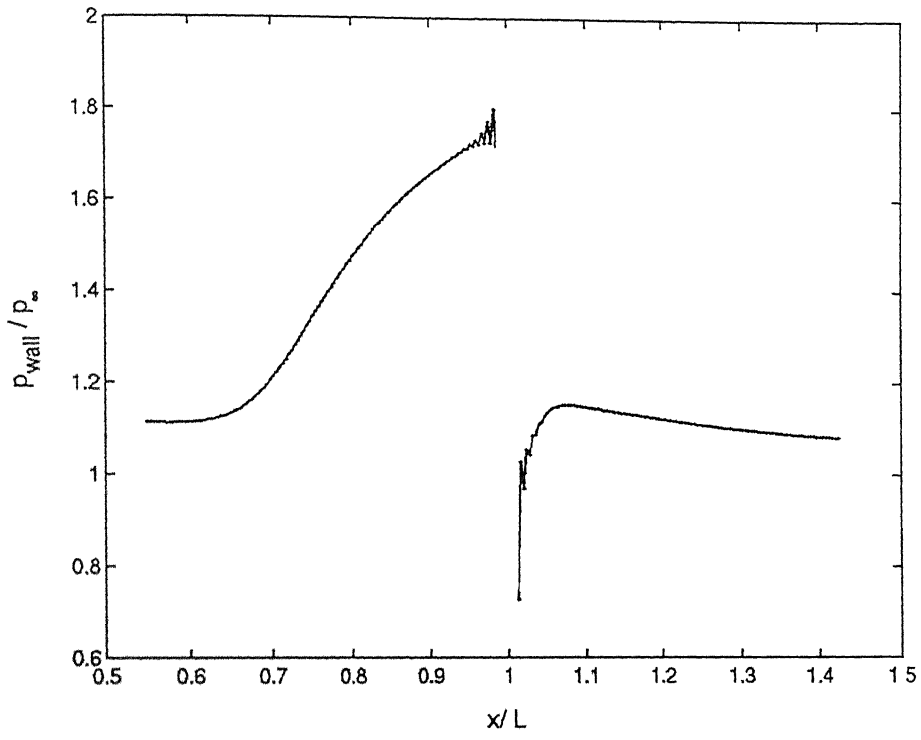

Figure 4.1: Comparison of Computed Surface pressure distribution with Ref. [13]

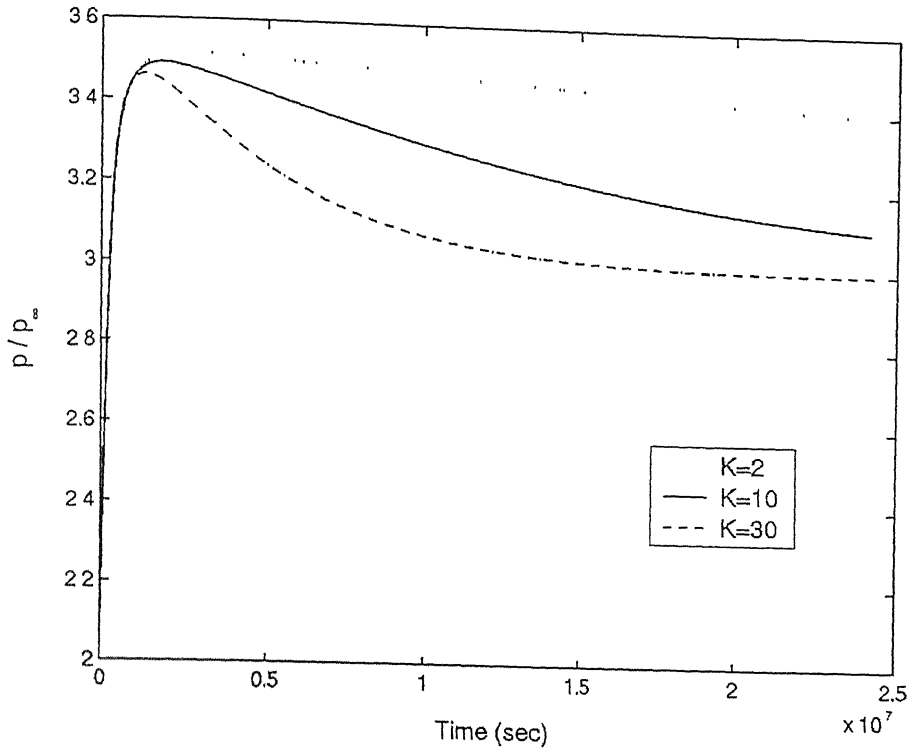

Figure 4.2: Variation of pressure ratio with time for $p_d / p_\infty = 3.0$ and M=4.0

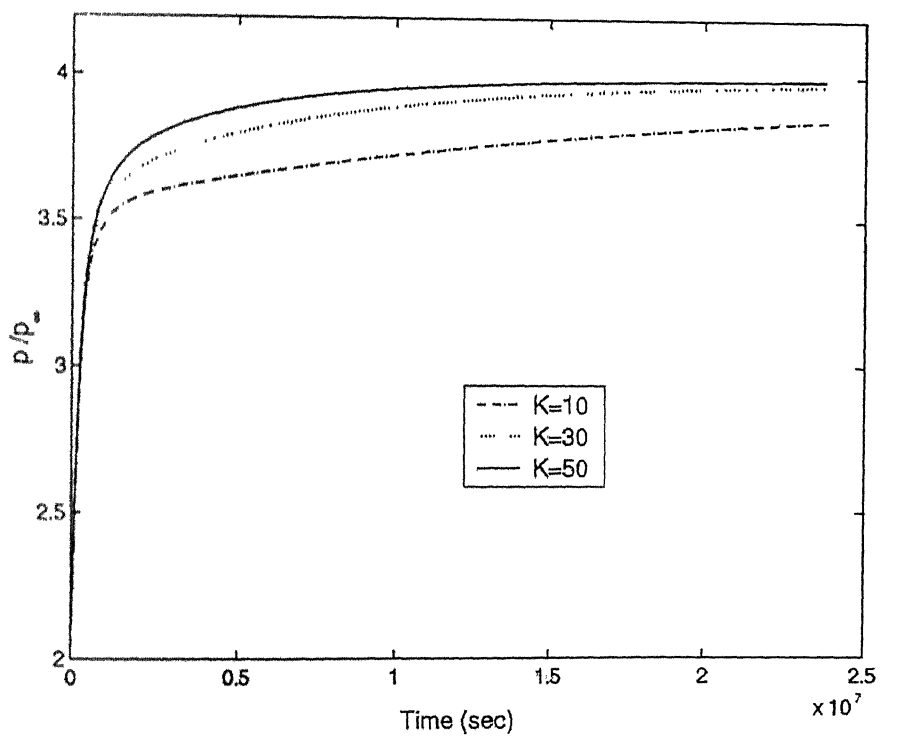

Figure 4.3: Variation of pressure ratio with time for $p_d / p_\infty = 4.0$ and M=4.0

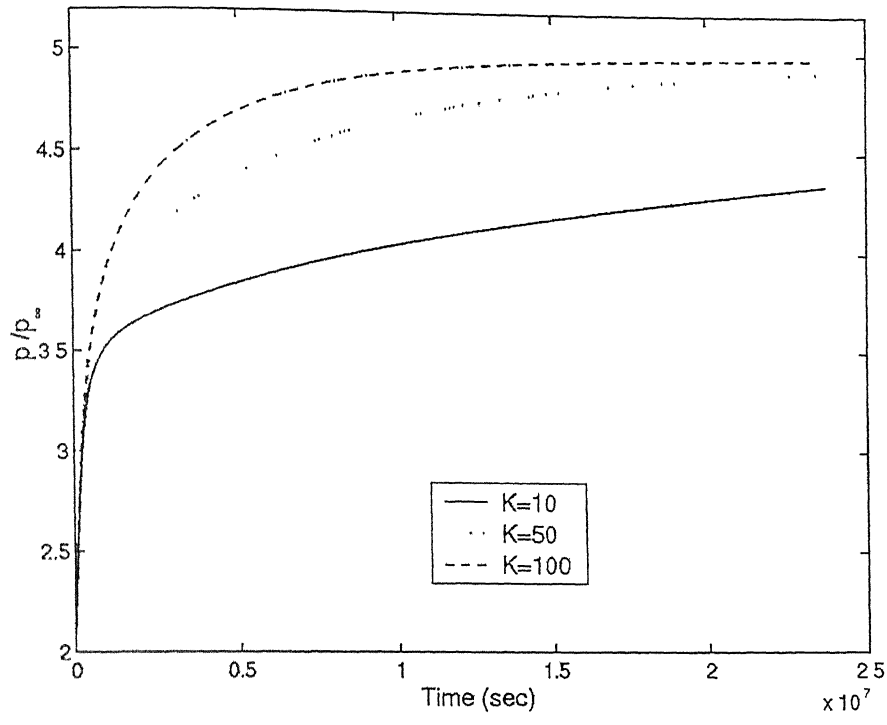

Figure 4.4: Variation of pressure ratio with time for $p_d / p_\infty = 5.0$ and M=4.0

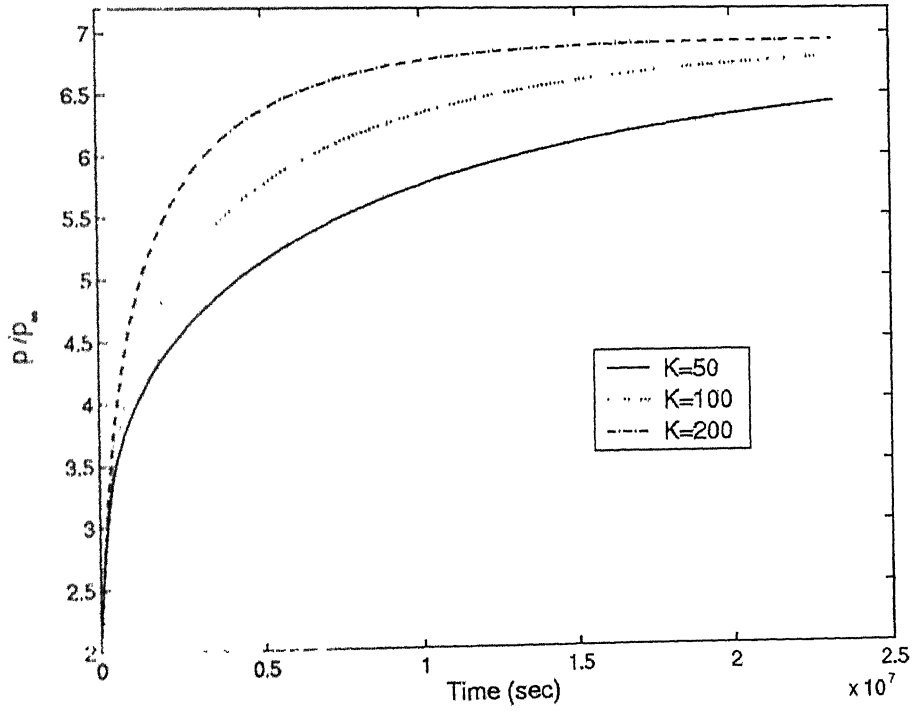

Figure 4.5: Variation of pressure ratio with time for $p_d / p_\infty = 7.0$ and M=4.0

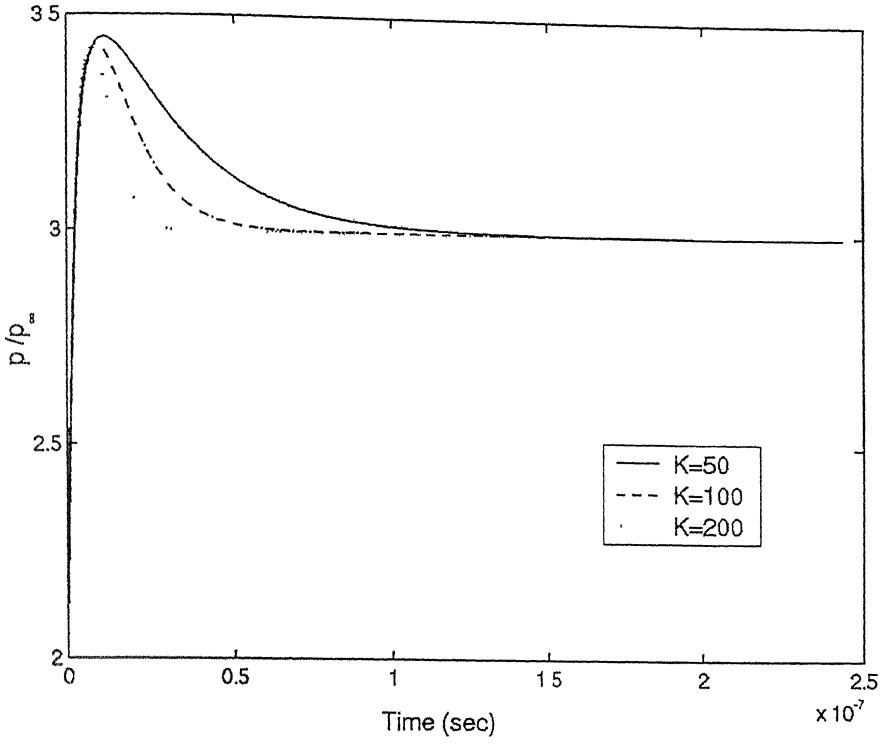

(a) Pressure ratio

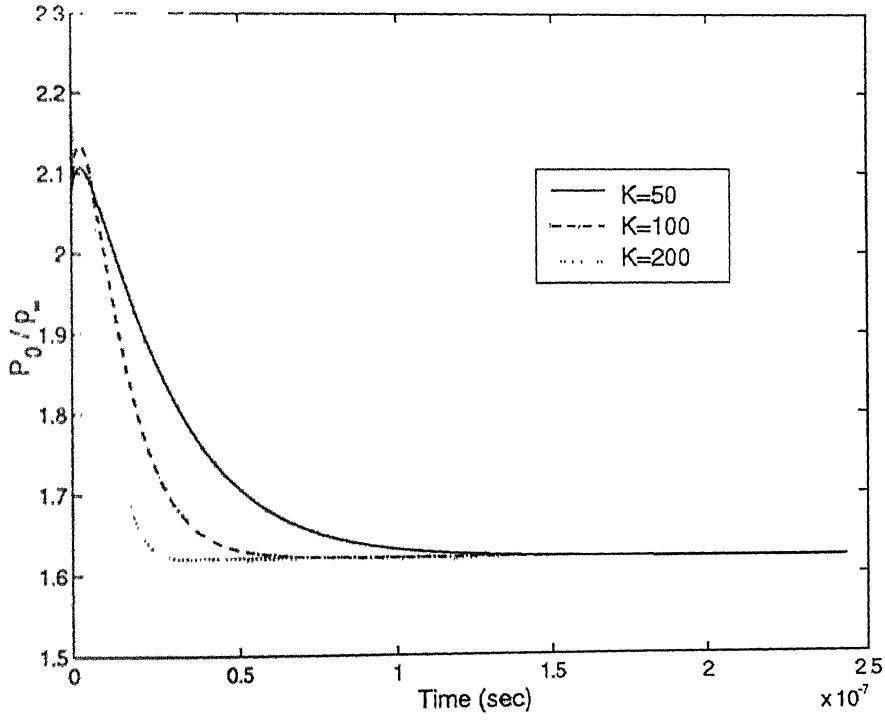

(b) Injection total pressure

Figure 4.6: Variation of different quantities with time for different K values and $p_d / p_\infty = 3.0$, M=4.0

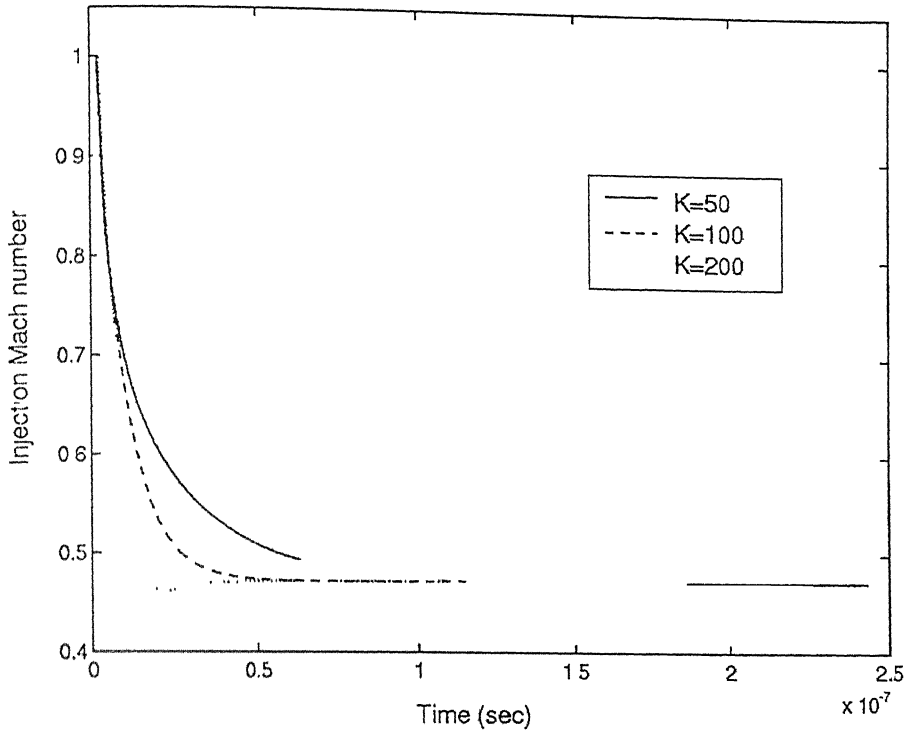

(c) Injection Mach number

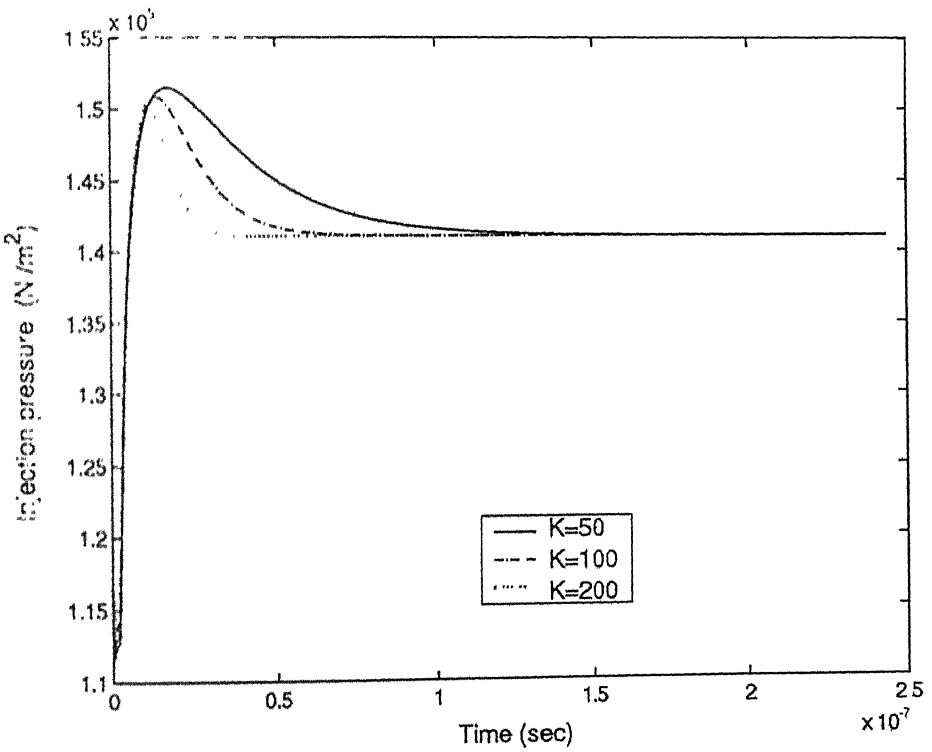

(d) Injection pressure

Figure 4.6: Variation of different quantities with time for different K values and $p_d / p_\infty = 3.0$, M=4.0

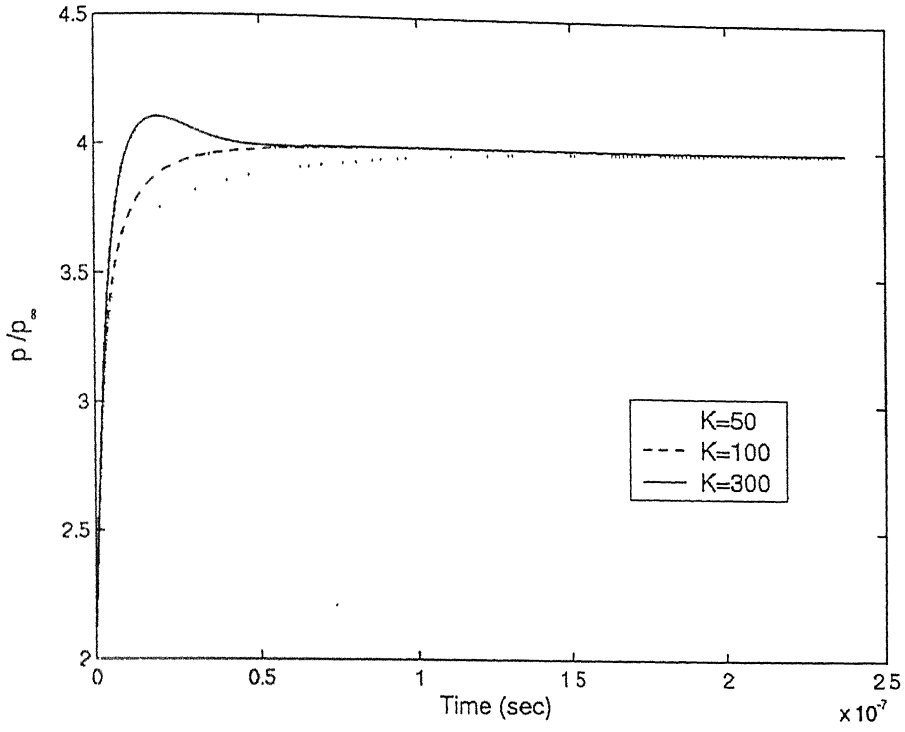

(a) Pressure ratio

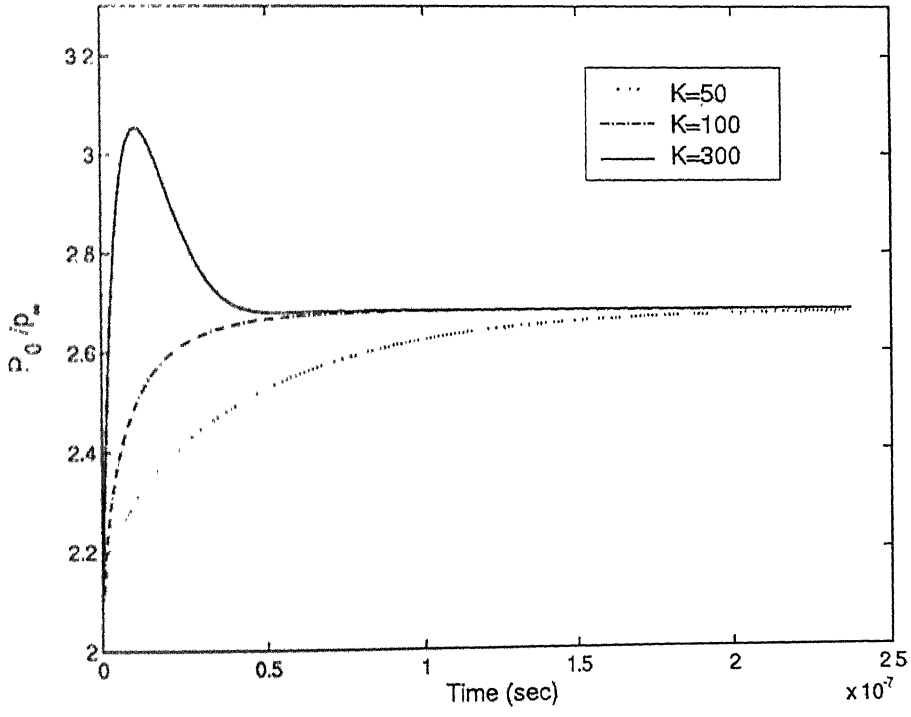

(b) Injection total pressure

Figure 4.7: Variation of different quantities with time for different K values and $p_d / p_\infty = 4.0$, M=4.0

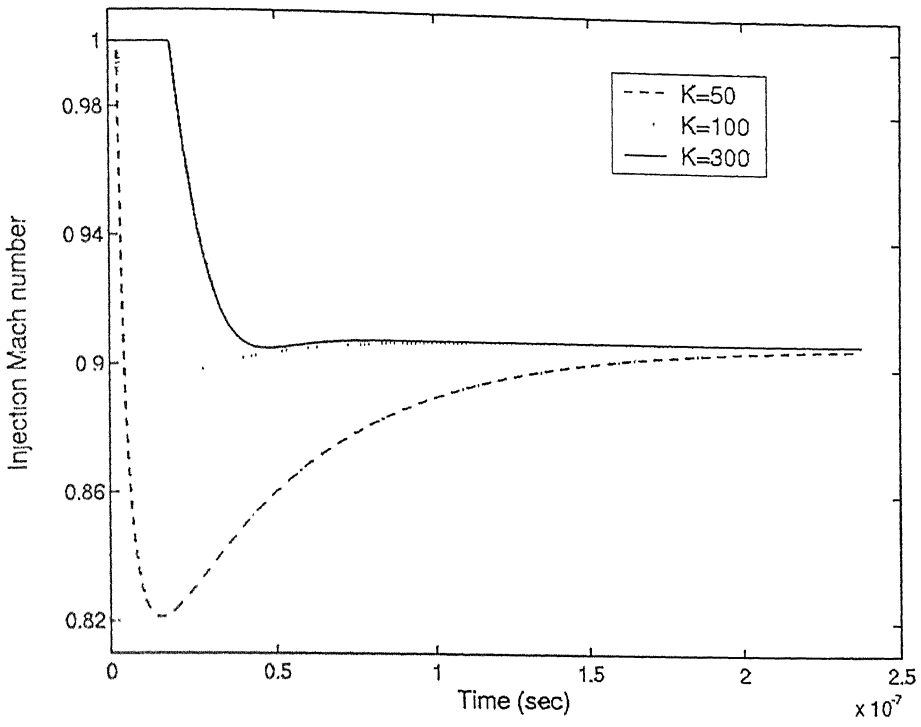

(c) Injection Mach number

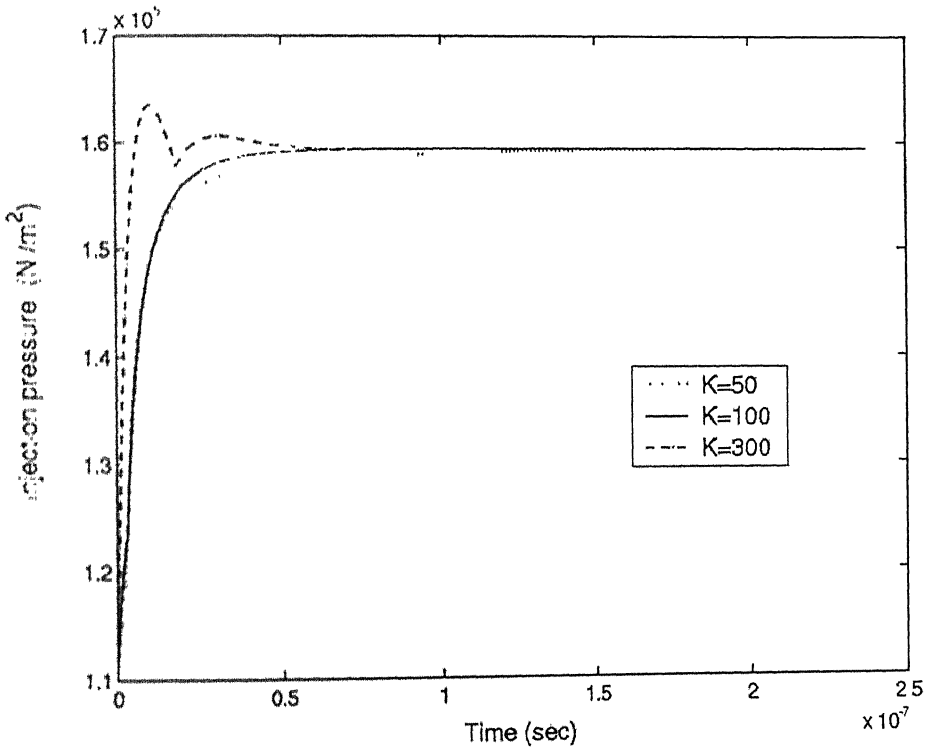

(d) Injection pressure

Figure 4.7: Variation of different quantities with time for different K values and $p_d / p_\infty = 4.0$, M=4.0

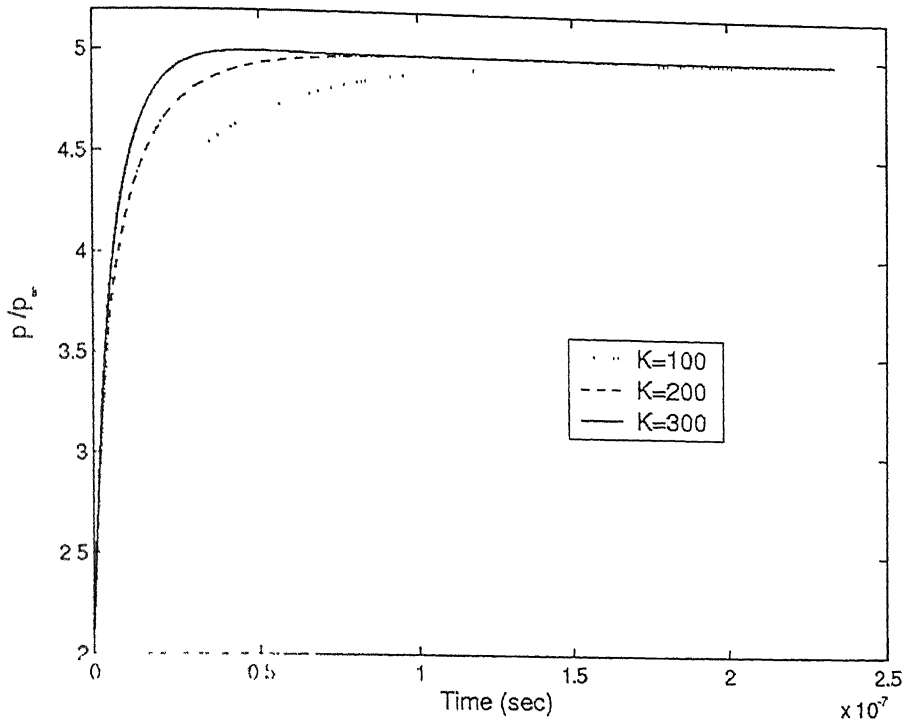

(a) Pressure ratio

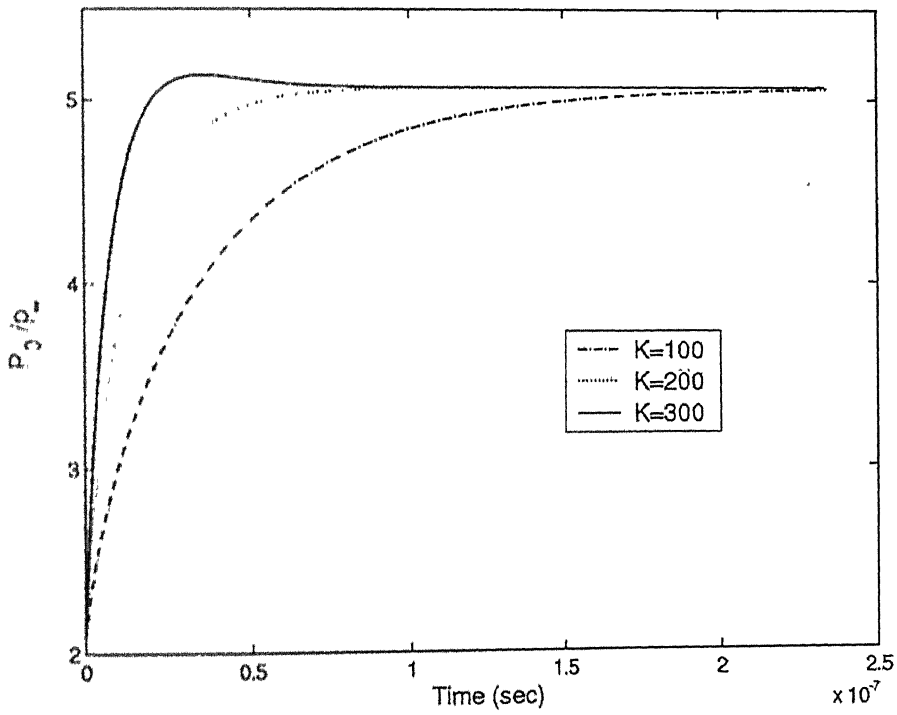

(b) Injection total pressure

Figure 4.8: Variation of different quantities with time for different K values and $p_d / p_m = 5.0$, M=4.0

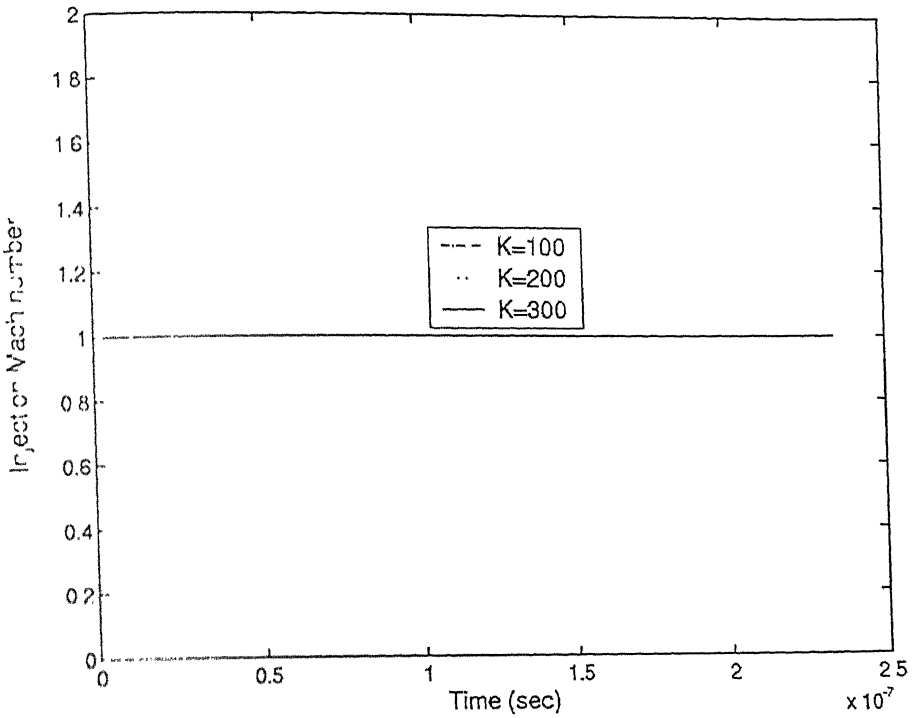

(c) Injection Mach number

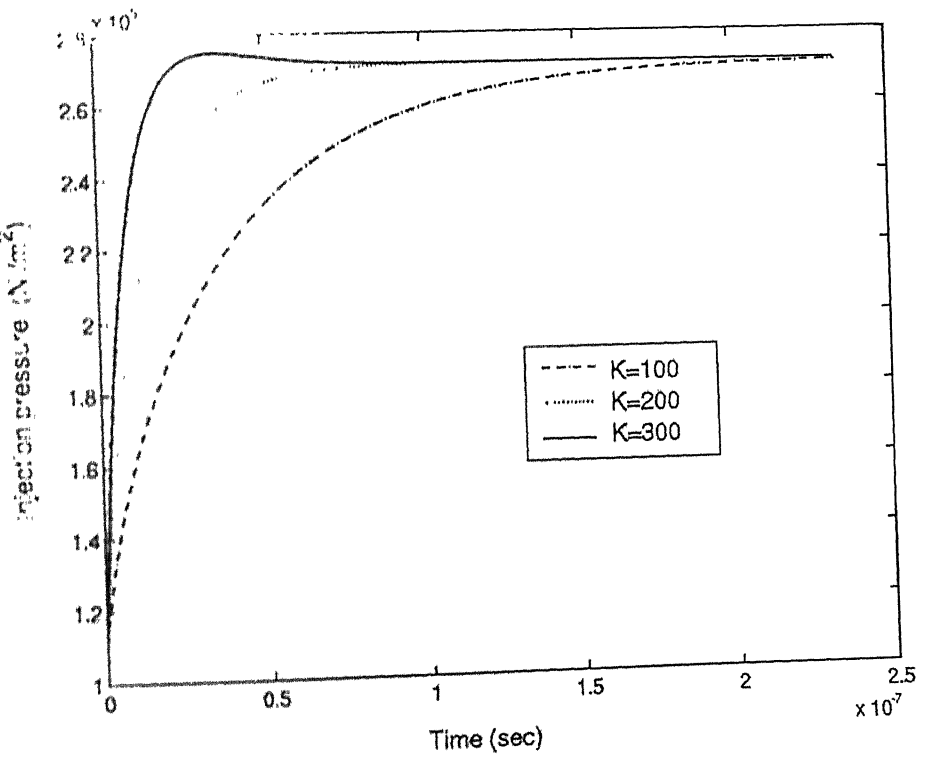

(e) Injection pressure

Figure 4.8: Variation of different quantities with time for different K values and $p_d / p_\infty = 5.0$, M=4.0

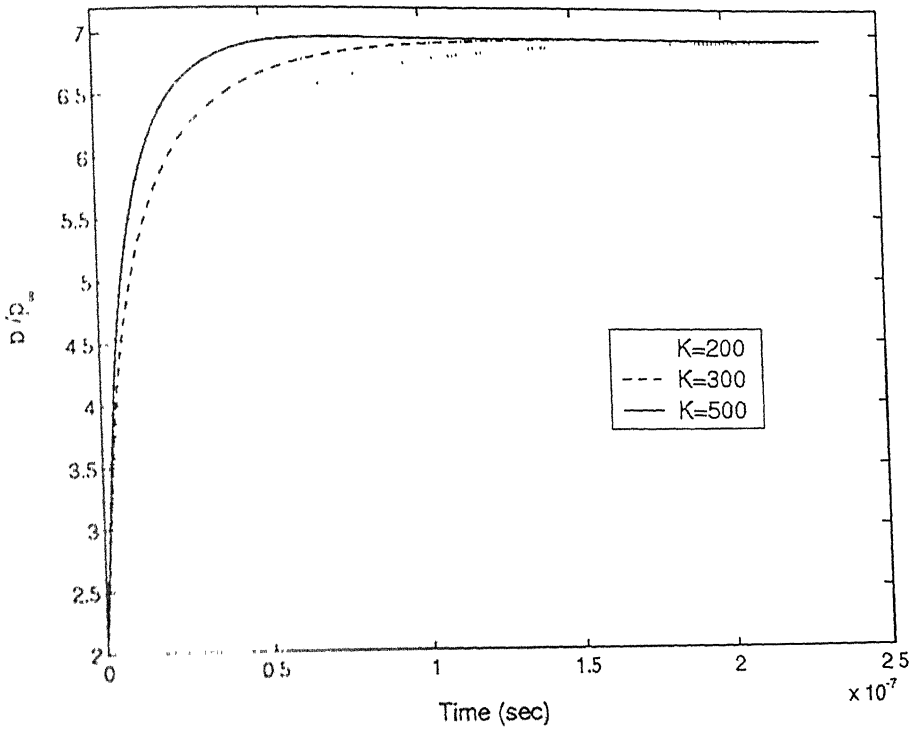

(a) Pressure ratio

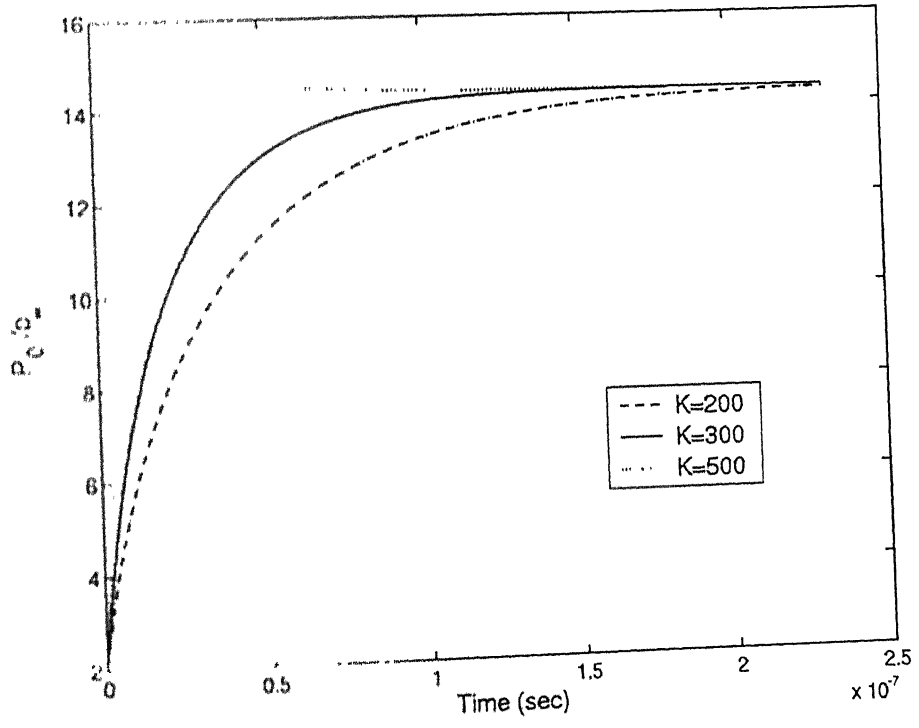

(b) Injection total pressure

Figure 4.9: Variation of different quantities with time for different K values and $p_d / p_{\infty} = 7.0$, M=4.0

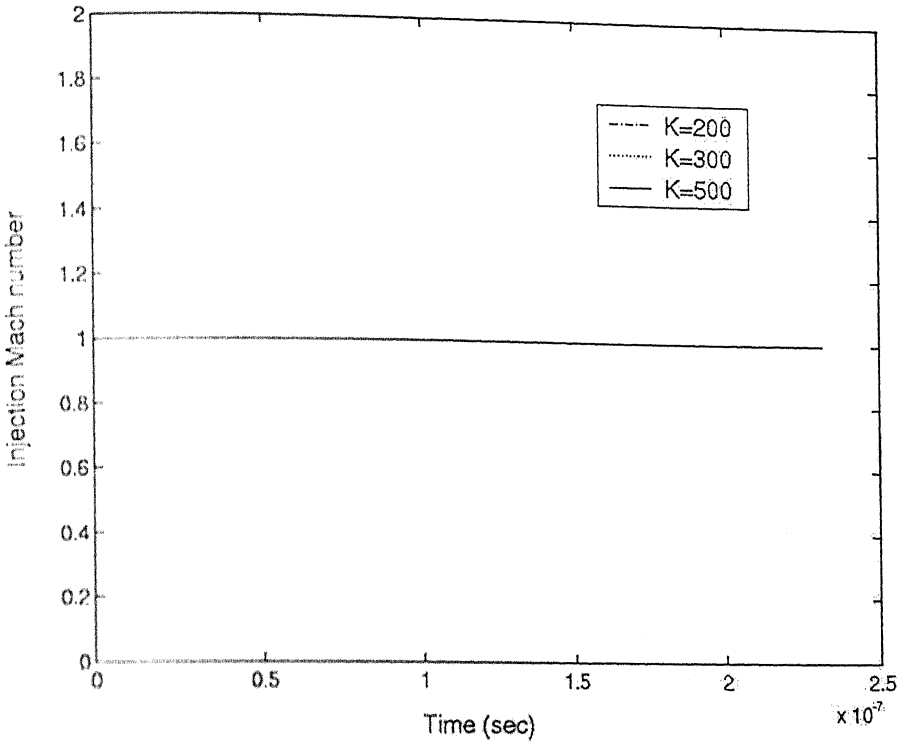

(c) Injection Mach number

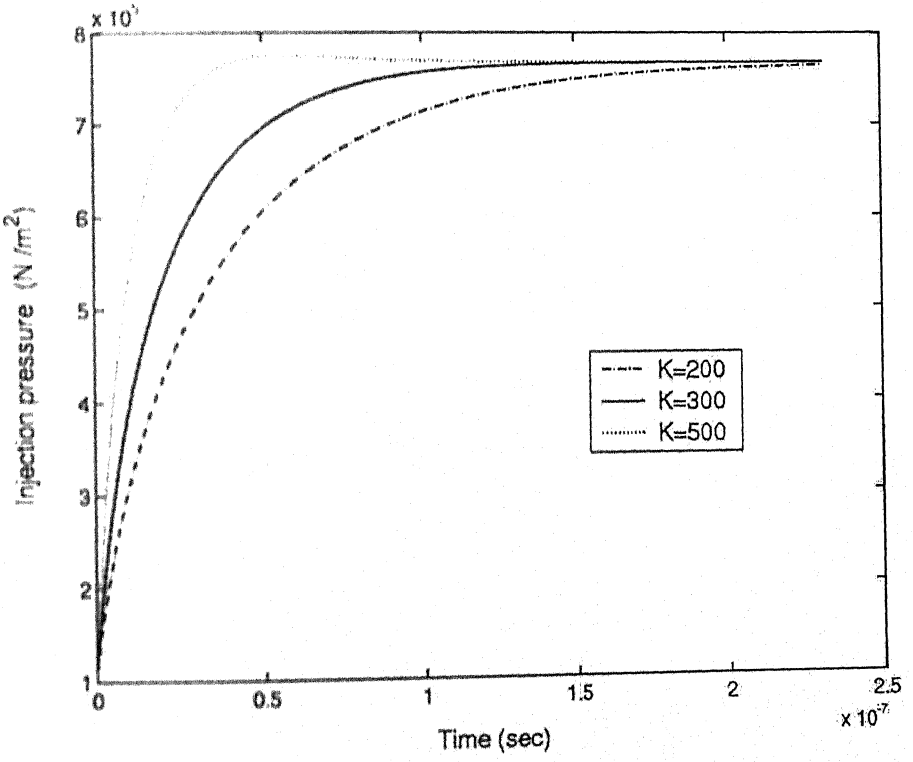

(d) Injection pressure

Figure 4.9: Variation of different quantities with time for different K values and $p_d / p_\infty = 7.0$, M=4.0

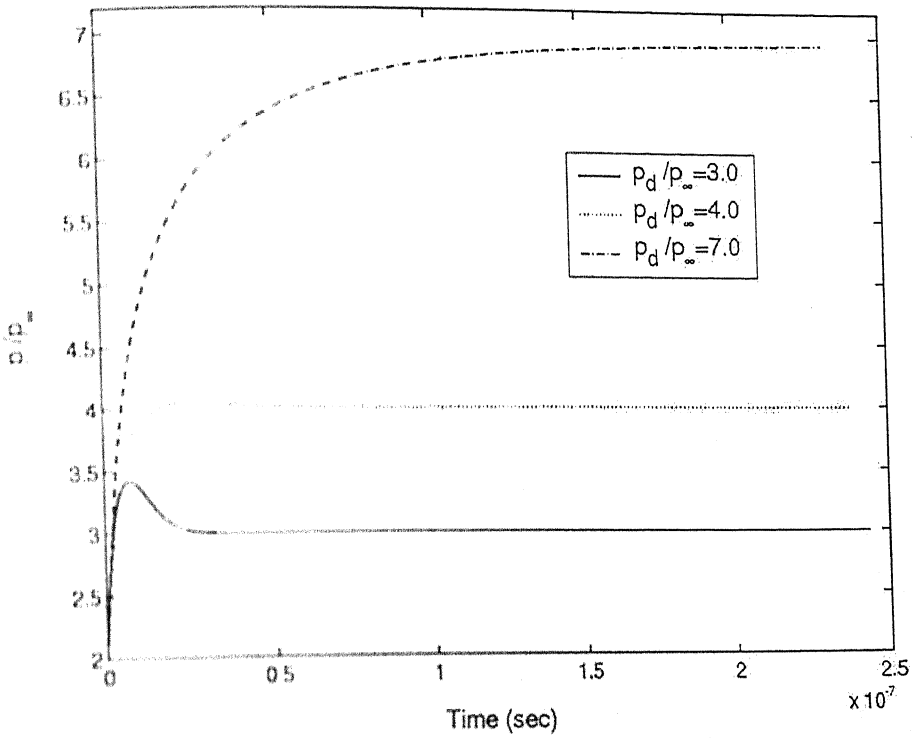

(a) Pressure ratio

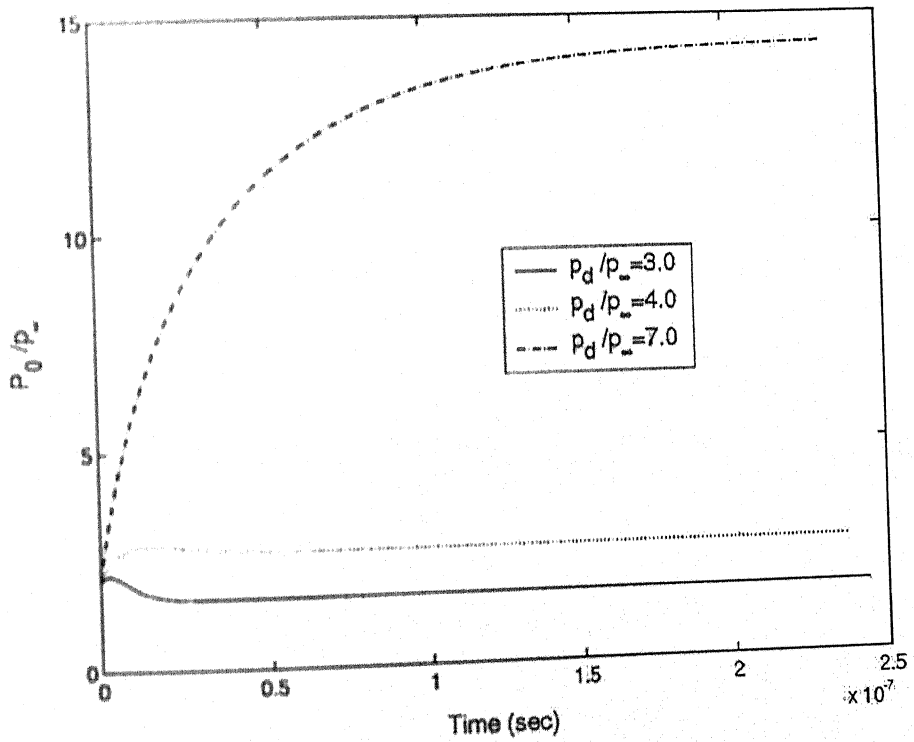

(b) Injection total pressure

Figure 4.10: Variation of different quantities with time for different desired pressure ratios and M=4.0, K=200

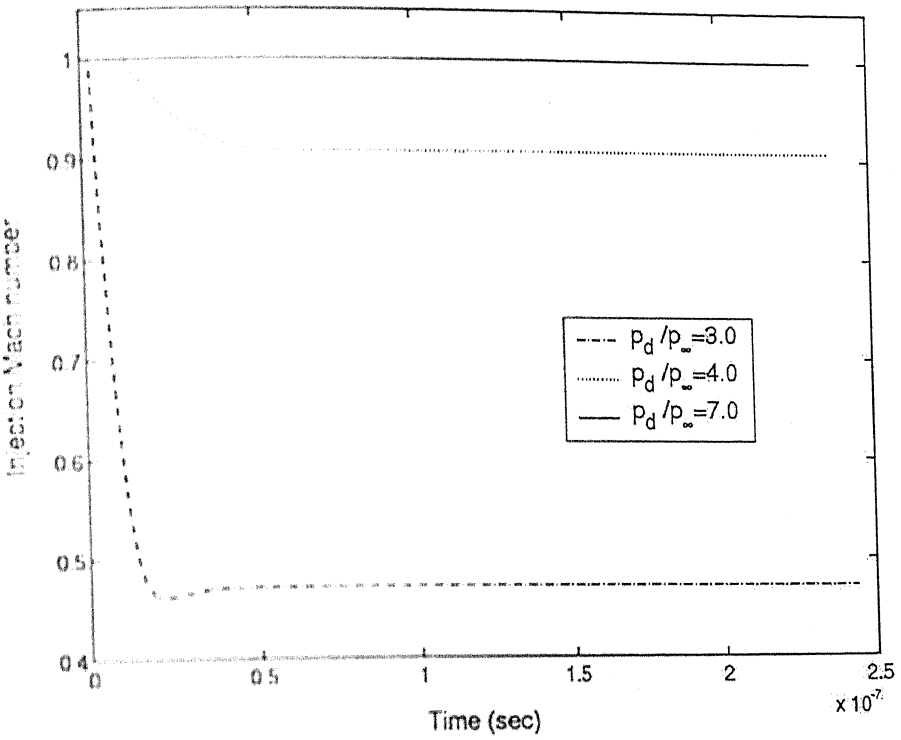

(c) Injection Mach number

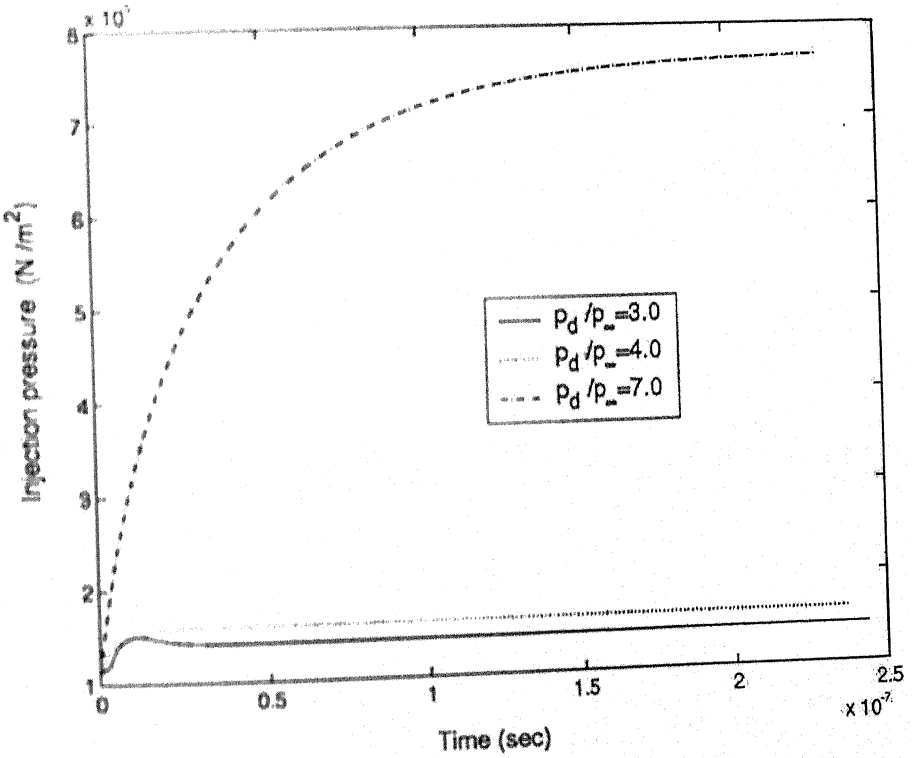

(d) Injection pressure

Figure 4.10: Variation of different quantities with time for different desired pressure ratios and M=4.0, K=200

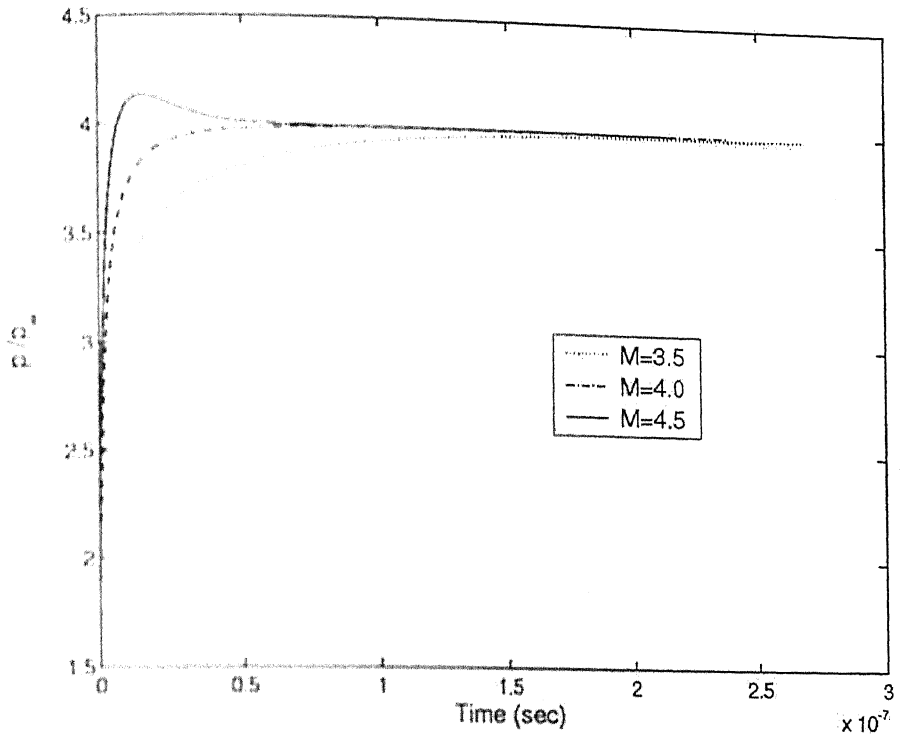

(a) Pressure ratio

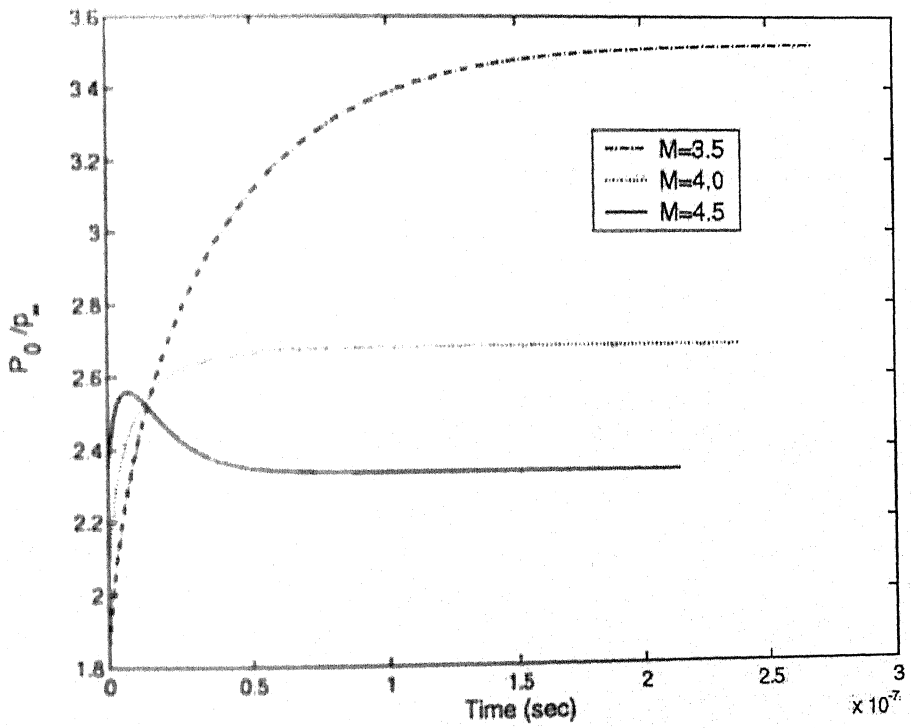

(b) Injection total pressure

Figure 4.11: Variation of different quantities with time for different Mach numbers and $p_d / p_\infty = 4.0$, K=100

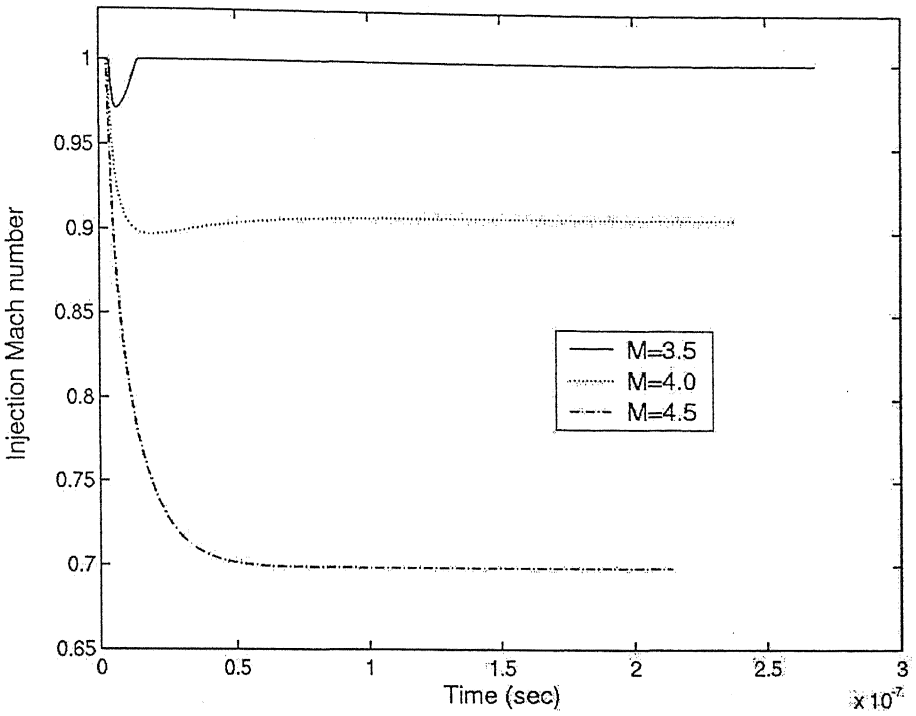

(c) Injection Mach number

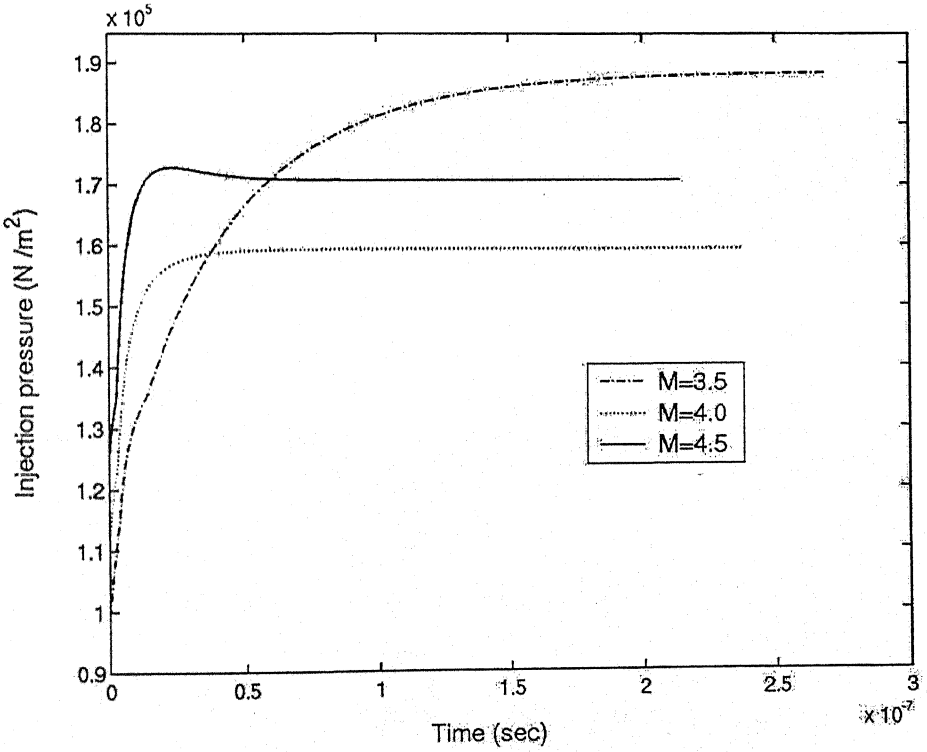

(d) Injection pressure

Figure 4.11: Variation of different quantities with time for different Mach numbers and $p_d / p_\infty = 4.0$, K=100

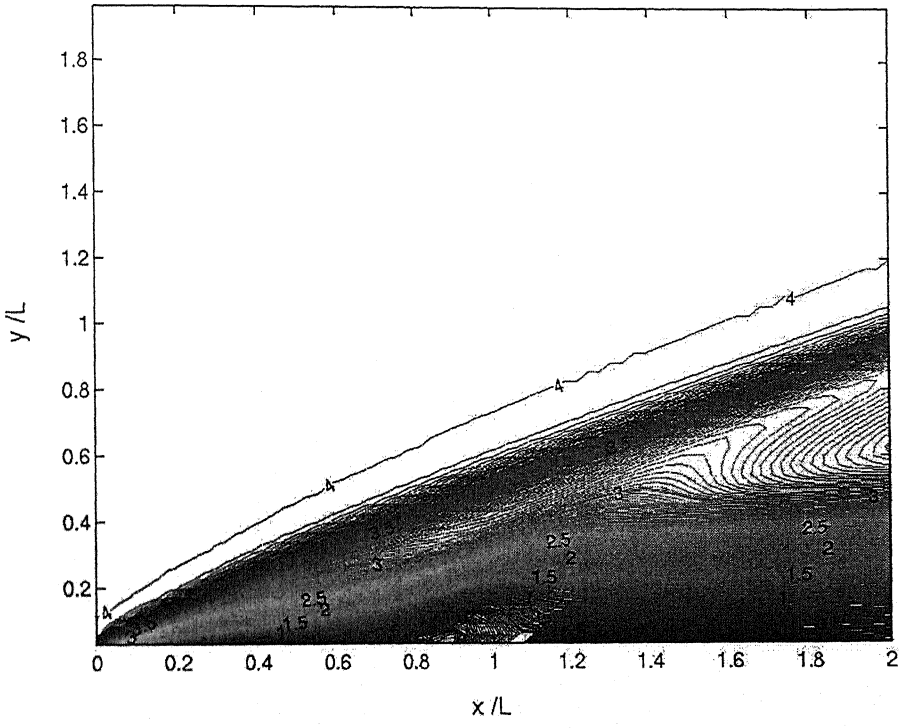

Figure 4.12: Mach number contours at a transient time (250 iterations) for M=4.0 $p_d / p_\infty = 4.0$ and K=100

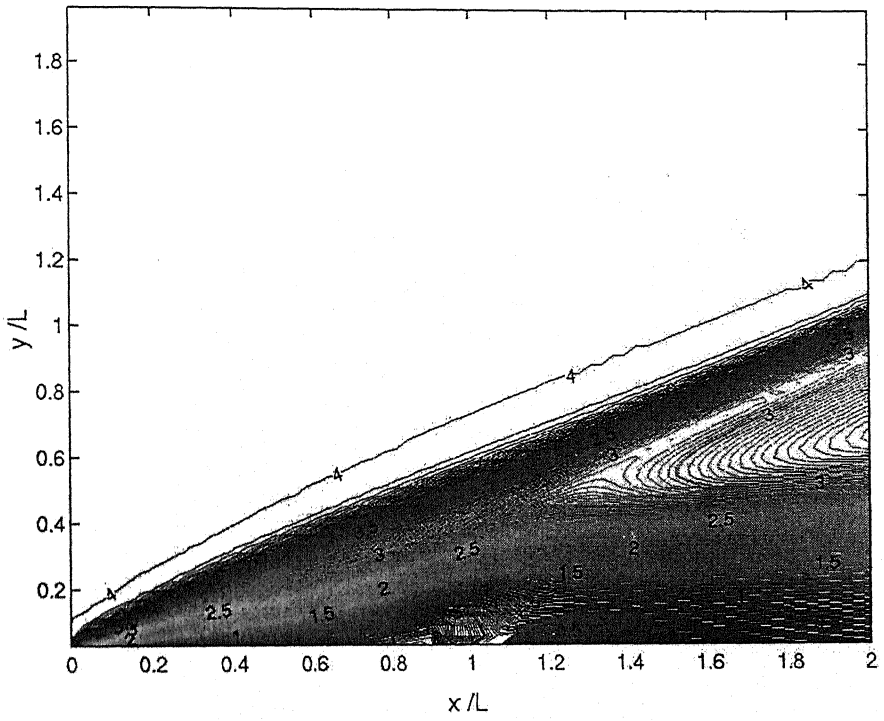

Figure 4.13: Mach number contours at steady state (7000 iterations) for M=4.0, $p_d / p_\infty = 4.0$, K=100

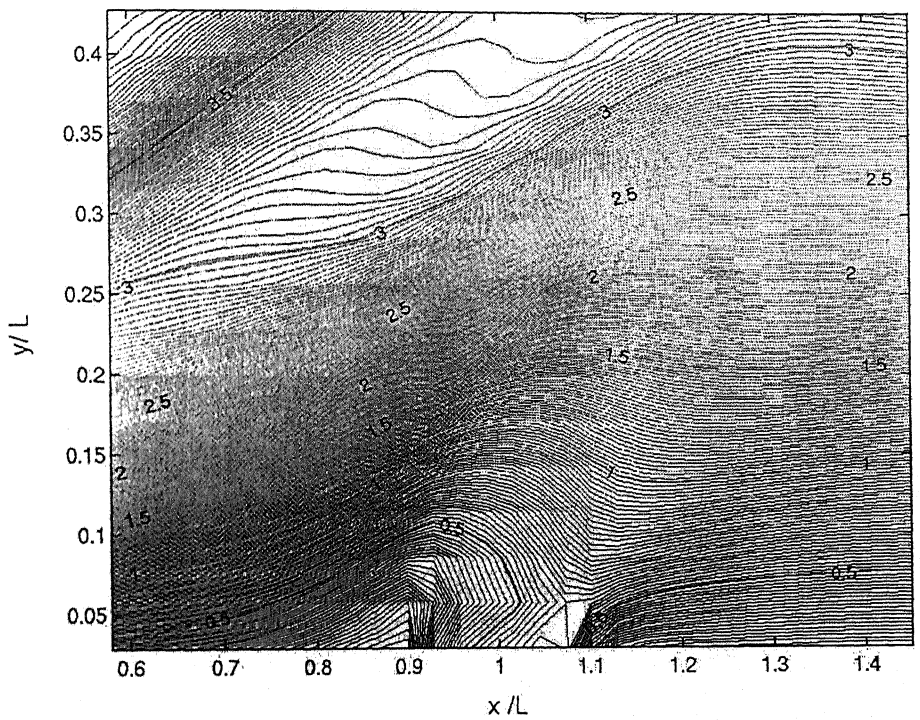

Figure 4.14: Mach number contours near the slot at a transient time (100 iterations) for M=4.0 $p_d / p_\infty = 4.0$ and K=100

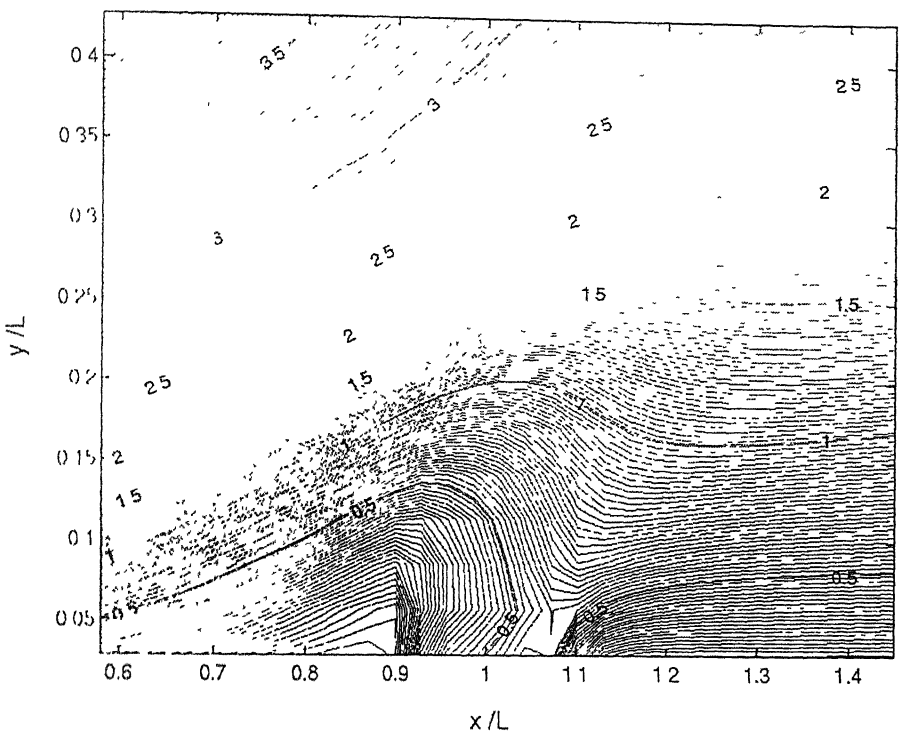

Figure 4.15: Mach number contours near the slot at steady state (7000 iterations) for M=4.0, $p_d / p_\infty = 4.0$ and K=100.

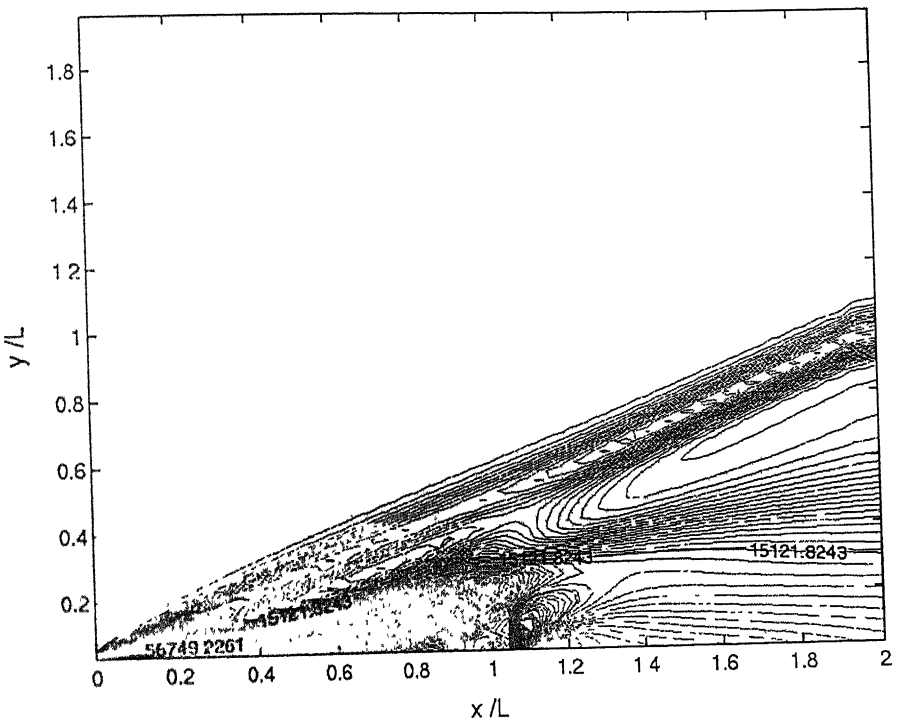

Figure 4.16: Shear stress τ_{xy} contours for M=4.0, $p_d / p_\infty = 4.0$, K=100

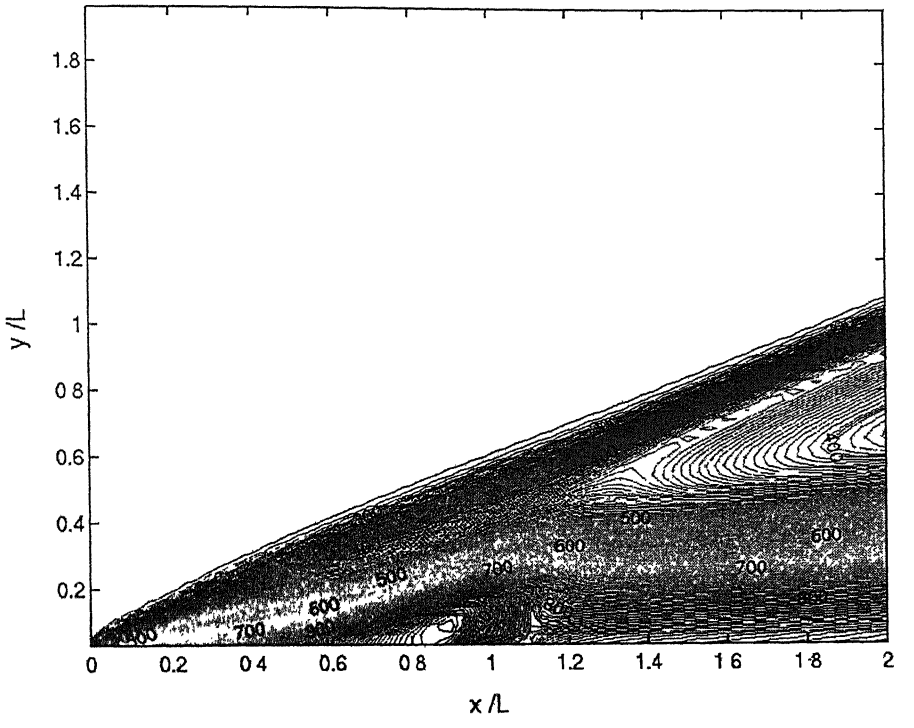

Figure 4.17: Temperature contours for M=4.0, $p_d / p_\infty = 4.0$, K=100

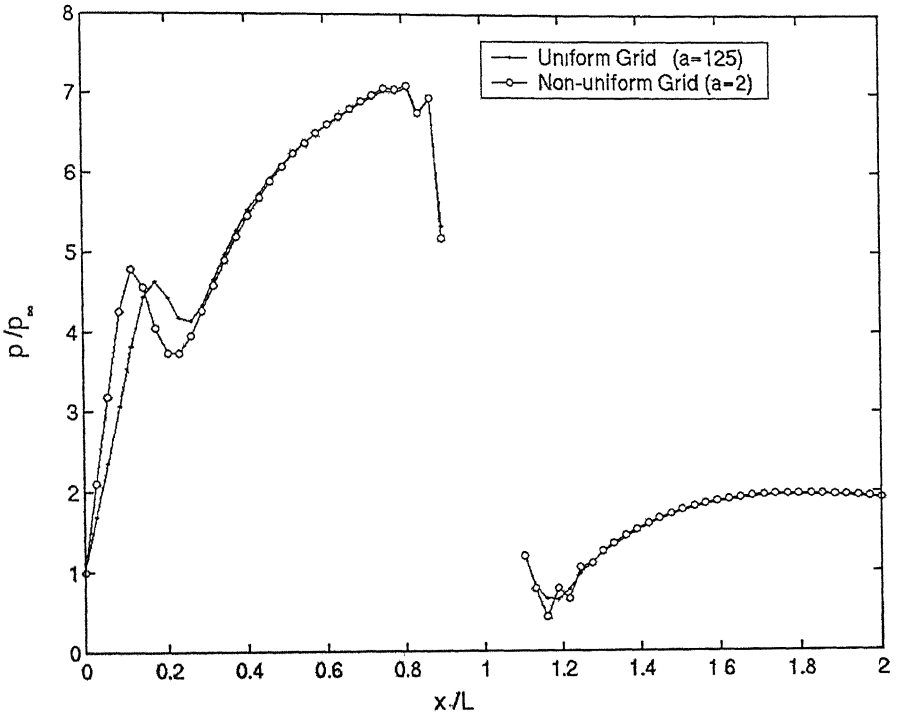

Figure 4.18: Comparison of surface pressure distribution for a Uniform and Non-uniform grid (70×70)

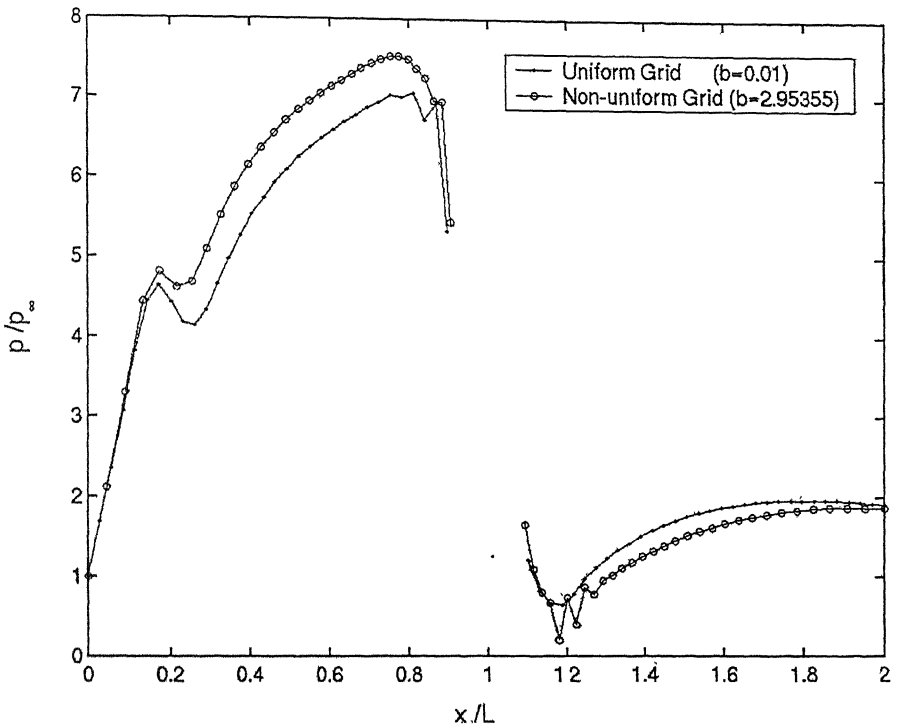

Figure 4.19: Comparison of surface pressure distribution for a Uniform and Non-uniform grid (70×70)

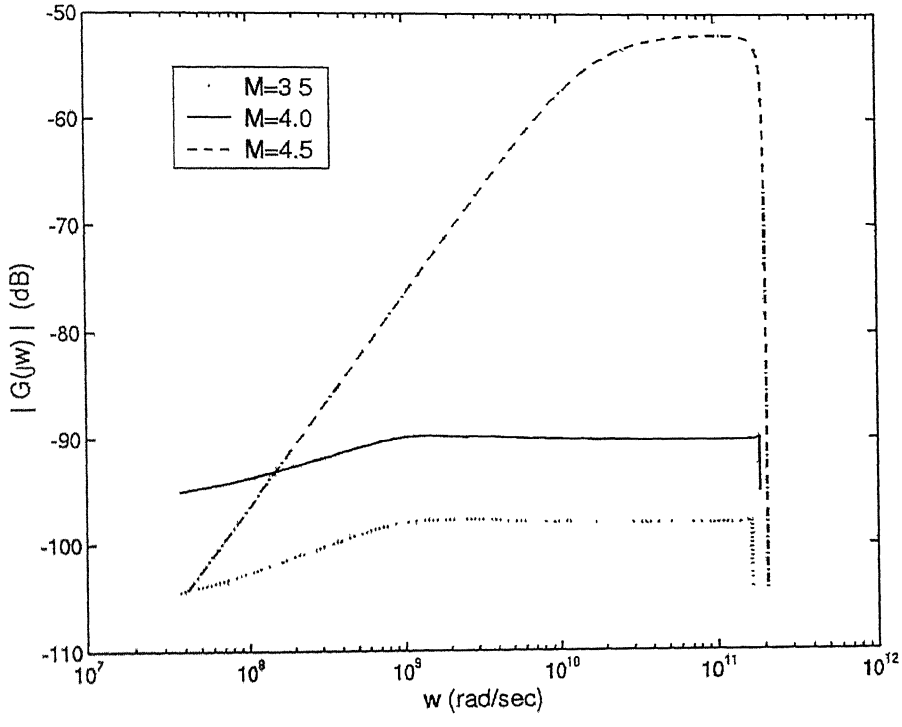

Figure 4.20: Fast Fourier Transform plots for different Mach numbers and $p_d / p_\infty = 4.0$, K=100

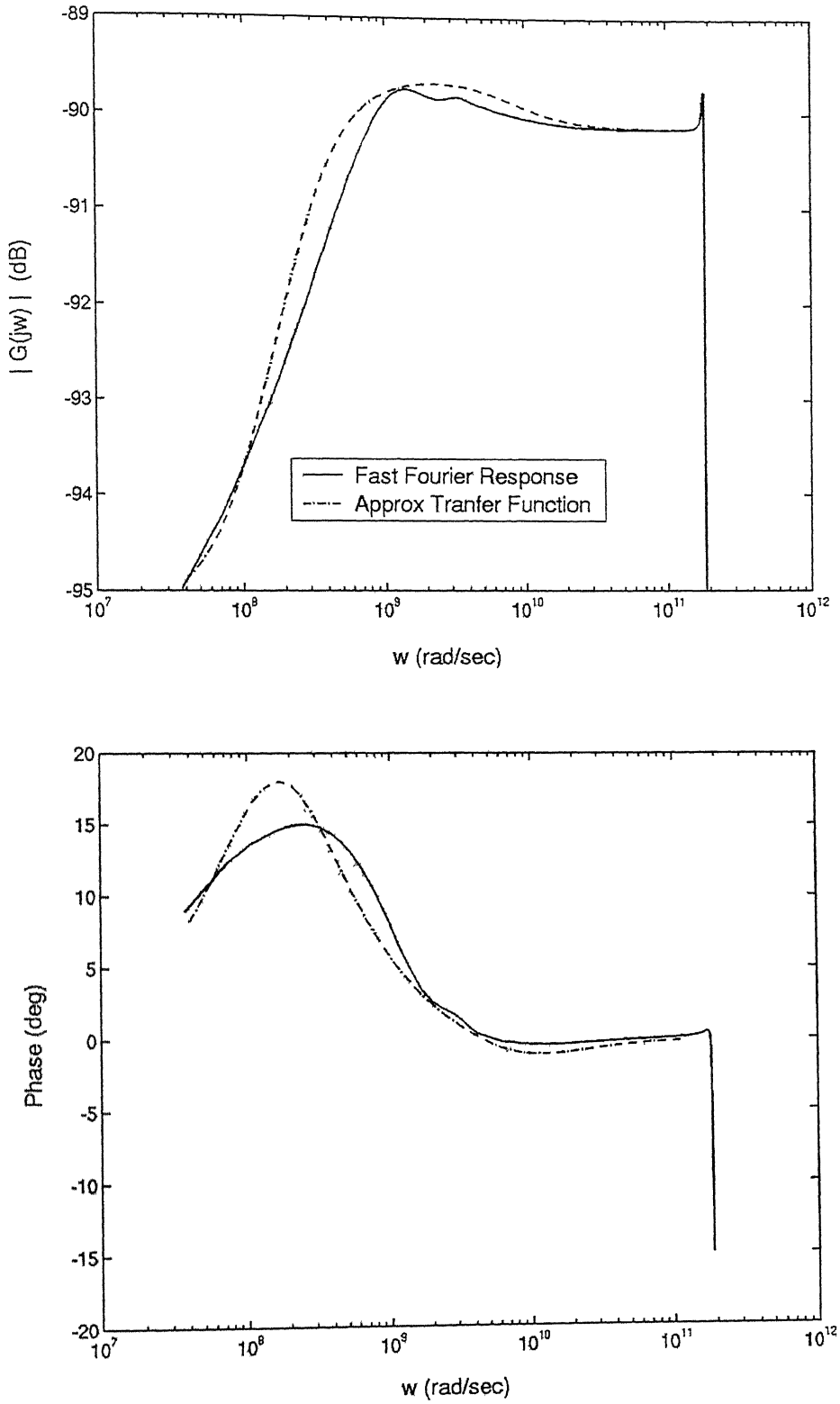

Figure 4.21: Comparison of Fast Fourier and Approximate Transfer function frequency response for M=4.0 $p_d / p_\infty = 4.0$, K=100

Chapter 5

Conclusions and Suggestions for Future work

5.1 Conclusions

A numerical study to design a linear feedback control system for the case of transverse injection over a flat plate in supersonic flow that gives a desired static pressure ratio upstream of the slot has been carried out by integrating the two-dimensional unsteady Navier-Stokes equations. Isentropic flow was assumed in the nozzle. The computed result was compared with a reference to check for its validation. The study has been performed for different desired static pressure ratios and controller constants. Results depicted that for same freestream Mach number, a higher desired pressure ratio requires greater secondary mass flow, which increases the strength of bow shock and thus giving a higher desired static pressure ratio. From the results, we can see that the nozzle doesn't need to be choked for some cases of desired pressure ratios thus showing the advantage of using an active feedback control system, as it requires an unchoked flow to get the desired pressure ratio. This is not the case with an open-loop control, used in all references where they always used a choked flow. Also such a control system gives the exact desired value even for small changes in freestream Mach numbers thus showing the robustness of system to small changes in freestream Mach numbers. The transfer function of the system has been

obtained for a particular case which can be used to improve the performance of control system by including a non-linear controller.

5.2 Future Scope of the Work

Much of scope exists for extending this work. The control system designed finds its application in scramjet engine where there is considerable importance of the maximum pressure for mixing enhancements of fuel and air and also in thrust vector regulation. The same concept of controlling pressure can be extended to control heat transfers for cooling the surfaces and controlling skin friction for drag reduction in re-entry vehicles.

The controller design in this thesis was carried out by numerical experimentation. But, the controller design can also be carried out by transfer function approach. Once the transfer function of the system is obtained about an equilibrium point, the same can be used to design the controller, which can be an extension of this thesis. The code can also be extended to include the turbulence modeling for the case of turbulent flows and also can be extended for a three-dimensional problem, by including the third spatial parameter. The code can be made more accurate by including non-equilibrium effects when solving the problem in a higher Mach number range.

References

[1] William H. Dorrance, "Viscous Hypersonic Flow", McGraw-Hill Book company, Inc., 1962.

[2] Spaid, F.W., Zukoski, E.E., "Secondary Injection of Gases into a Supersonic Flow," *AIAA Journal*, Vol.2, No.10, 1964, pp. 1689-1696.

[3] Spaid, F.W., Zukoski, E.E., "Further Experiments Concerning Secondary Injection of Gases into a Supersonic Flow," *AIAA Journal*, Vol.4, No.12, 1966, pp. 2216-2218.

[4] Schetz, J.A., Billig, F.S., "Penetration of Gaseous Jets Injected into a Supersonic Stream," *Journal of Spacecraft and Rockets,* Vol.3, No.11, 1966, pp. 1658-1665.

[5] George Lee, "Hypersonic Flow over a Blunt Flat plate with Surface Mass Transfer," *AIAA Journal,* Vol.4, No.11, 1966, pp. 2049-2051.

[6] Spaid, F.W., Zukoski, E.E., "A Study of the Interaction of Gaseous Jets from Transverse Slots with Supersonic External Flows," *AIAA Journal*, Vol.6, No.2, 1968, pp. 205-212.

[7] Spaid, F.W., "Two Dimensional Jet Interaction Studies at Large Values of Reynolds and Mach Numbers," *AIAA Journal*, Vol.13, No.11, 1975, pp. 1430-1434.

[8] Napolitano, M., "Numerical Study of Strong Slot Injection into a Supersonic Laminar Boundary Layer," *AIAA Journal*, Vol.18, No.1, 1980, pp. 72-77.

[9] Weidner, E.H., Drummond, J.P., "Numerical Study of a Scramjet Engine Flow field," *AIAA Journal*, Vol.20, No.9, 1982, pp. 1182-1187

[10] Weidner, E.H., Drummond, J.P., "Numerical Study of Staged Fuel Injection for Supersonic Combustion," *AIAA Journal*, Vol.20, No.10, 1982, pp. 1426-1431.

[11] Rizzetta, D.P., "Numerical Simulation of Slot Injection into a Turbulent Supersonic Stream," *AIAA Journal*, Vol.30, No.10, 1992, pp. 2434-2439.

[12] Aso, S., Okuyama, S., Kawai, M., Ando, Y., "Experimental Study on Mixing Phenomena in Supersonic Flows with Slot Injection," AIAA Paper 91-0016, Jan. 1991.

[13] Chenault, C.F., Beran, P.S., "K-ε and Reynolds Stress Turbulence Model Comparisons for Two-dimensional Injection Flows," *AIAA Journal*, Vol.36, No.8, 1998, pp. 1401-1412.

[14] Michael Kenworthy and Schetz J.A., "Experimental study of Slot Injection into a supersonic stream," *AIAA Journal,* Vol.11, No.5, 1973, pp. 585-587.

[15] Inger, G.R. and Swean, T.F., "Vectored Injection into Laminar Boundary Layers with Heat transfer," *AIAA Journal,* Vol.13, No.5, 1975, pp. 616-622.

[16] Nilson, R.H. and Tsuei, Y.G., "Film Cooling by Oblique Slot Injection in High-speed Laminar Flow," *AIAA Journal,* Vol.13, No.9, 1975, pp. 1199-1202.

[17] Schetz, J.A., vanOvereem, J., "Skin Friction Reduction by Injection through combinations of Slots and Porous sections," *AIAA Journal*, Vol.13, No.8, 1975, pp. 971-972.

[18] Inger, G.R. and Swean, T.F., "Hypersonic Viscous-Inviscid Interaction with Vectored surface Mass Transfer," *AIAA Journal*, Vol.14, No.5, 1976, pp. 589-596.

[19] Hefner, J.N., "Effect of Geometry Modifications on Effectiveness of Slot Injection in Hypersonic Flow," *AIAA Journal*, Vol.14, No.6, 1976, pp. 817-818

[20] Brandeis, J., "Influence of Finite slot size on Boundary layer with Suction or Injection," *AIAA Journal*, Vol.21, No.4, 1983, pp

[21] O'Connor, J.P., Haji-Sheikh, A., "Numerical Study of Film Cooling in Supersonic Flow," *AIAA Journal*, Vol.31, No.10, 1992, pp. 2426-2433.

[22] Dershin, H., Leonard, C.A., Gallaher, W.H., "Direct Measurement of Skin Friction on a Porous Flat plate with Mass Injection," *AIAA Journal*, Vol.5, No.11, 1967, pp. 1934-1939.

[23] Thomas, P.D., "Flow over a Finite plate with massive injection," *AIAA Journal,* Vol.7, No.4, 1969, pp. 681-687.

[24] Clark, K.J., Vardo, C.T., Jaffe, N.A. and Covington, M.A., "Cooling by Discrete and Porous Injection into a Turbulent, Supersonic Boundary Layer," *AIAA Journal,* Vol. 12, No.12, 1974, pp. 1679-1686.

[25] El-Mistikawy, T.M., and Werle, M.J., "Numerical Method for Boundary Layers with Blowing – The Exponential Box Scheme," *AIAA Journal,* Vol.16, No.7, 1978, pp. 749-750.

[26] Catalin Nae, "Unsteady Flow control using Synthetic Jet Actuator," AIAA paper –2000–2403, Fluids 2000 conference and Exhibit, Denver, CO, June 19-22, 2000.

[27] Calkins, F.T., Mabe, J.H., "Multilayer PVDF actuators for Active Flow Control," AIAA paper 2001-1560, Structural Dynamics, and Materials conference and Exhibit, 42nd, Seattle, WA, April 16-19, 2001.

[28] Vakili, A.D., Sauerwein, S.C., Miller, D.N., "Pulsed Injection applied to nozzle internal flow control," AIAA, Aerospace sciences Meeting and Exhibit, 37th, Reno, NU, January 11-14, 1999.

[29] Gaitonde, D.V., Poggie, J., "Simulation of Magnetogasdynamic Flow control Techniques," AIAA paper 2000-2326, Fluids 2000 conference and Exhibit, Denver, CO, June 19-22, 2000.

[30] Lineberry, J.T., Rosa, R.J., Bityurin, V.A., Botcharov, A.N., Potebnya, "Prospects of MHD Flow control for Hypersonics," AIAA paper 2000-3057, Intersociety Energy Conversion Engineering conference and Exhibit (IECEC), 35th, Las Vegas, NV, July 24-28, 2000.

[31] Luc Leger, Eric Moreau, Gerard Touchard, "Electro hydrodynamic airflow control along a flat plate by a DC surface Corona discharge – Velocity profile and wall pressure measurements," AIAA 2002-2833, 1st Flow control conference, 24-26 June 2002, St. Louis, Missouri.

[32] Riggins, D.W., Nelson, H.F., "Hypersonic Flow Control using Upstream Focused Energy Deposition," AIAA, Aerospace sciences Meeting and Exhibit, 37th, Reno, NU, January 11-14, 1999.

[33] Yutaka Ikeda, "Real Time Active Flow Control based on Modern Control Theory," AIAA 98-2911, AIAA, Fluid Dynamics conference, 29th, Albuquerque, NM, June 15-18, 1998.

[34] Anderson, D.A., Tannehill, J.C., Pletcher, R.H., "Computational Fluid Mechanics and Heat Transfer," McGraw-Hill, New York, 1984, Chap. 5,9.

[35] John D. Anderson Jr., "Computational Fluid Dynamics," *The Basics with Applications*, International Editions, 1995, McGraw-Hill Inc., New York.

[36] Hoffmann, K.A. and Chiang, S.T., "Computational Fluid Dynamics, Volume I", Engineering Education System, 1998.

[37] Ogata, K., "Modern Control Engineering," 3rd ed., Prentice-Hall, New Delhi, 2000, pp. 471-504.

[38] Benjamin C. Kuo, "Automatic Control Systems", Prentice Hall of India Pvt. Ltd., 5th Ed., 1989.

[39] Ashish Tewari, "Modern Control Design with MATLAB and SIMULINK", John wiley and sons, UK, 2002.

[40] Shailendra Mishra, "Navier-Stokes Computations for Two-dimensional Hypersonic Flow", M.Tech. Thesis, IIT Kanpur, December 1998.